2016

# Anisotropic Electrical Response of Carbon Fiber Reinforced Composite Materials

Mohammad Faisal Haider
*University of South Carolina*

# ANISOTROPIC ELECTRICAL RESPONSE OF CARBON FIBER REINFORCED COMPOSITE MATERIALS

by

Mohammad Faisal Haider

Bachelor of Science
Bangladesh University of Engineering & Technology, 2009

Master of Science
Bangladesh University of Engineering & Technology, 2011

---

Submitted in Partial Fulfillment of the Requirements

For the Degree of Master of Science in

Mechanical Engineering

College of Engineering and Computing

University of South Carolina

2016

Accepted by:

Prasun K. Majumdar, Director of Thesis

Victor Giurgiutiu, Reader

Lacy Ford, Senior Vice Provost and Dean of Graduate Studies

## DEDICATION

This work is dedicated to my wife, Farzana Yasmeen, who has been a constant source of support and encouragement during the challenges of my life. This work is also dedicated to my parents, and brothers, who have always loved me unconditionally and whose good examples have taught me to work hard for the things that I aspire to achieve.

## ACKNOWLEDGEMENTS

I would like to thank my MS Thesis advisor Dr. Prasun K. Majumdar for guiding and supporting me over the years. I am thankful to him for his advice, many insightful discussions and suggestions. His composite classes helped me to learn about multi-scale degradation mechanisms, durability and remaining life estimate. He introduced me first in the area of Broadband Dielectric Spectroscopy.

I would also like to express my sincere gratitude to Professor Victor Giurgiutiu, reader of this thesis. His encouraging words, positive way of thinking, patience, motivation, enthusiasm, and immense knowledge motivates me throughout the day. I am very grateful to him that he agreed to guide me as my PhD advisor also. I got him as my PhD advisor at the very important stage of my life. It would have been impossible for me to proceed so far without his support. All the knowledge and skills I have learned so far from him, he will be an invaluable treasure for my whole life.

I want to thank Professor Kenneth Reifsnider for his advice many times during my research study, serving in my qualifying exam committee, and also for providing access to the state of the art facilities of the SOFC center. A special thanks to Dr. Rassel Raihan and Dr. Fazle Rabbi for helping me to get trained on experimental facilities. I am really grateful to Stephanie Angeloni, Hunter Goman and Kevin Epley for running tremendous amount of experiments for me. I also appreciate the help of my colleagues, Mr. Lee Woolley, Jon-Michael Adkins, Jeffrey Baker and Vamsee Vadlamudi during my research work.

## ABSTRACT

Composites materials are often subjected to multi-physical conditions in different applications where, in addition to mechanical loads, they also need to sustain other types of loads such as electrical currents. The multi-physical behavior of composites needs to be understood and analyzed to facilitate new multi-functional material design. An essential first step towards this goal is to understand how multi-physics properties depend on local details (e.g. micro-structure). Composite materials have heterogeneous electrical properties (carbon/epoxy) at the local level that can be different at the global level. To conduct the multi-physics study, the electrical signal is employed to the composite sample for conducting coupled thermal-electrical-mechanical analysis. Anisotropic electrical behavior is measured experimentally and threshold of nonlinear behavior has been quantified. The electrical-thermal response is studied with thermography tests and finite element analysis. Their results are compared to understand the role of distributed microstructural damage.

The durability and damage tolerance of composite materials for both mechanical and electrical loads also need to be studied. Although the durability of composite materials under mechanical loading has been studied over several decades, their response to electrical currents is still not fully understood. On the one hand, the electrical response of the composite changes with the evolution of damage due to mechanical loads. On the other hand, the stages of damage evolution in composite laminates under mechanical loading can be clearly effected by electrical loading. This thesis investigates how existing damage due

to prior mechanical loading history may grow when subjected to subsequent electrical currents. The behavior is multi-physical with interplay of mechanical damage and thermal behavior resulting from Joule heating by electrical current. Results show that anisotropy in electrical response heavily depends on material state consisting of evolving damage. A 3D X-ray tomography has been used to visualize damage and validate experimental observations.

A micromechanics model has been developed to further assist understanding of the anisotropic nature of composite materials at the micro scale. The effective anisotropic electrical conductivity of composites is strongly affected by many parameters including volume fractions, distributions, and orientations of constituents. Given the electrical properties of the constituents, one important goal of micromechanics of materials consists of predicting electrical response of the heterogeneous material on the basis of the geometries and properties of the individual constituents. An effective electrical conductivity estimation is performed by using classical micromechanics techniques (concentric cylinder method or CCM) that investigate the effect of the fiber/matrix electrical properties and their volume fractions on the micro scale composite response.

## TABLE OF CONTENTS

## LIST OF FIGURES

# CHAPTER 1
# INTRODUCTION

Heterogeneous materials, consist of clearly distinguishable constituents (or phases) that show different properties. Multifunctional composites have anisotropic properties that can be tailored for a particular application. Such advanced "engineered materials" are increasingly used in a wide range of applications (mechanical, civil or aerospace structures; energy devices such as fuel cells, batteries; and bio-medical components) and have the potential to evolve in even more complex heterogeneous formulations to meet the needs of the 21st century. Carbon fiber reinforced polymer (CFRP) composites are one class of such engineered materials which has historically provided outstanding mechanical properties in a light weight design, led to many technological revolutions, and has recently attracted renewed interest because of its incorporation in the primary structures of major commercial aircraft. Despite progress in analysis and fabrication of composite material systems, their long term performance is currently an area of active research [1]-[10]. On the other hand, relatively little attention has been given to their other physical properties, which in parallel affected their use in electrical applications. One should not forget that insulating materials or dielectrics show various properties at different voltages, temperatures, frequencies, moisture content, and mechanical stresses. These should be considered in the design as well as in the diagnostics [11].

Composite materials are traditionally designed for use as structural materials. The traditional approach to the development of structures is to address the load-carrying

function and other functional requirements separately, resulting in a suboptimal load-bearing structure with add-on attachments which perform the non-structural functions with the penalty of added weight. Recently, however, there has been increased interest in the development of load-bearing materials and structures which have integral non-load-bearing functions, probably guided by discoveries about how multifunctional biological systems work. Commonly investigated non-structural functions include electrical and/or thermal conductivity, sensing and actuation, energy harvesting/storage, self-healing capability, electromagnetic interference (EMI) shielding, recyclability and biodegradability [12]. The major difference in property requirements between structural composites and electronic composites is that the design criteria for these two groups of composites are different. While structural composites emphasize high strength and high modulus, electronic composites emphasize high thermal conductivity, low thermal expansion, low dielectric constant, high/low electrical conductivity and/or electromagnetic interference (EMI) shielding effectiveness, depending on the particular multifunctional application. Low density is desirable for both aerospace structures and aerospace electronics [13]. However composites in electrical application can use expensive fillers, such as silver particles, or conductive silver paste which serve to provide high electrical conductivity with penalty of added weight. Such an approach is not desire in structural composites. So, for a true multi-functional composite material development, the inherent synergy of above functional properties and core structural behavior must be understood. The electrical properties of the system (i.e. its conductivity and dielectric permittivity) are influenced by the properties of the constituents, interaction between them and geometrical configuration [14]-[20].

Damage tolerance in relation to lightning strikes is now an important engineering problem related to composite aircraft structures [21]-[24]. Electrical behavior of composites has attracted increased interest to understand reliability under electrical effects and also to provide multi-functional performance (coupled structural-thermal-electrical) in different applications. Under electrical load, electrical effects are often coupled with structural integrity and thermal behavior due to "Joule heating" in composites and their joints. This multi-physical action leads to damage growth and ultimately affect the electrical response. An essential first step is to understand how multi-physics properties depend on evolution of damage. On the one hand, the multi-physics responses of the system are influenced by the properties of the constituents, interaction between them, and geometrical configuration [18]-[20]. On the other hand, the stages of damage evolution in composite laminates under mechanical loading can be clearly effected later by the electrical loading. The damage state can be represented by adopting a suitable electrical response. This thesis reports the thresholds limits of irreversible damage in carbon fiber composites due to electrical currents. This also investigates how existing damage due to prior mechanical loading history may grow when subjected to subsequent electrical currents. This inherently multi-physical behavior needs to be understood and analyzed to facilitate new multi-functional material design.

An essential first step towards this goal is to understand how multi-physics properties (e.g. electrical conductivity) depend on local details (e.g. micro-structure). This thesis will explore how electrical current is related to anisotropic material architecture and damage development. AC conductivity measurements were carried out in directions perpendicular, parallel, and at varying angles to the fiber axis. The microstructure was

characterized by 3D X-ray imaging system. The dependence of the frequency and the temperature upon conductivity has been, likewise, investigated. It is also shown that the high degree of fiber orientation is consistent with the conspicuous anisotropic behavior of the electrical conductivity. This will form a very basic foundation for a multi-functional material design.

A micromechanics model has been developed to further assist understanding of the anisotropic nature of composite materials at lamina level. Electrical conductivity of composites is affected by volume fractions, distributions, and orientations of constituents. Given the electrical properties of the constituents, one important goal of micromechanics of materials consists of predicting electrical response of the heterogeneous material on the basis of the geometries and properties of the individual phases. There are only few reports available on the micromechanics model for predicting electrical properties of composite materials.

In this study an effective electrical conductivity estimation is performed by using classical micromechanics techniques (composite cylinder assemblage method) that investigates the effect of the fiber/matrix electrical properties and their volume fractions on the micro scale composite response. Micromechanics schemes such as the Mori-Tanaka method, the Self-Consistent Method are good approximation methods for composites with a low volume fraction of reinforcements in a resin. Fiber reinforcements can be considered inclusions in the resin matrix. These treatments assume that one single inclusion is embedded into an infinite domain and that each inclusion is far enough apart to neglect their interactions [25]. Composite cylinder assemblage method (CCM) is an analytical

theory that is based on the assumption that composites are in a state of periodic arrangement.

In this thesis, Chapter Two gives an overview and literature review of the progressive failure of the composite materials, state of the art detection techniques and a description of characterization of material state. In Chapter Three there is a short discussion about the major experimental facilities that were used during this research. Chapter Four presents the results of the nonlinear electrical response of anisotropic electrical conductive carbon fiber reinforced polymer composites. Chapter Five discusses damage tolerance and interdependency of durability of woven carbon fiber composite materials under electrical and mechanical load. Chapter Six describes multi physics modeling of composite materials including the electrical potential distribution, current density and the thermal study. Chapter Seven presents micromechanics model for predicting anisotropic electrical conductivity of carbon fiber composite materials with interphase.

# CHAPTER 2
# LITERATURE REVIEW

## 2.1 STRUCTURE AND PROPERTIES OF COMPOSITES

A composite is a structural material that consists of two or more constituents that are combined at a macroscopic level and are not soluble in each other. One constituent is called the reinforcing phase and the one in which it is embedded is called the matrix. The reinforcing phase material may be in the form of fibers, particles, or flakes. The matrix phase materials are generally continuous. Examples of composite systems include concrete reinforced with steel and epoxy reinforced with graphite fibers, etc.

In many cases, using composites is more efficient. For example, in the highly competitive airline market, one is continuously looking for ways to lower the overall mass of the aircraft without decreasing the stiffness and strength of its components. This is possible by replacing conventional metal alloys with composite materials. Even if the composite material costs may be higher, the reduction in the number of parts in an assembly and the savings in fuel costs make them more profitable. For example, the military fighter plane, F-22 com-missioned in 2005 uses about 25% composite materials by weight while Boeing has built its next generation passenger airplane (787) using composites at approximately half the material weight [26].

A composite lamina consists of two or more distinct materials, combined at the macroscopic level, to attain desired properties that could not be achieved by either of the

constituent materials alone. A laminate is constructed by stacking a number of such laminae in the direction of the lamina thickness (Figure 1). A laminate is a stack of laminae, with different fiber orientations, bonded together to attain desired properties. Laminates can be classified as symmetric, asymmetric, balanced, and unbalanced composites [27].

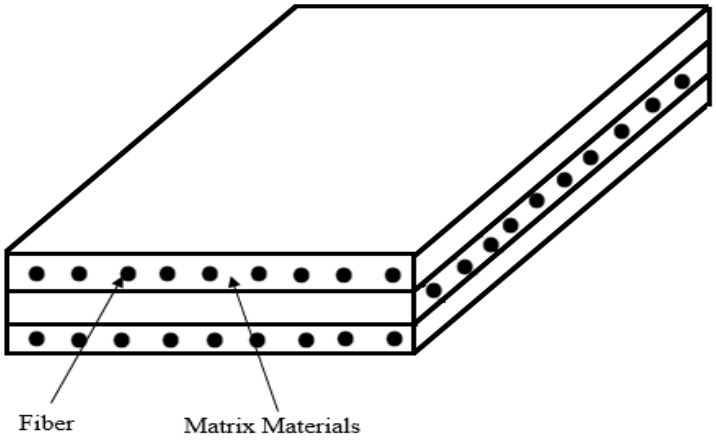


Figure 2.1 Typical laminate made of three laminae

A laminate is made of a group of single layers bonded to each other. Each layer can be identified by its location in the laminate, its material, and its angle of orientation with a reference axis (Figure 2.2).

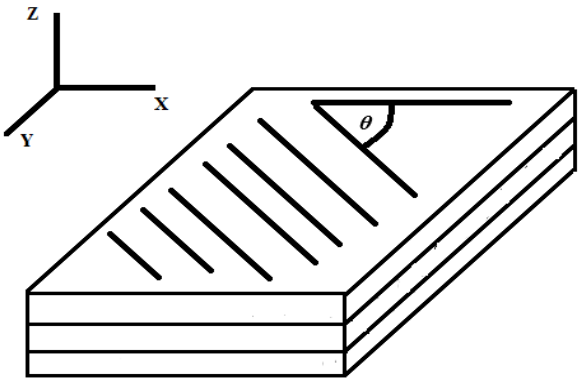


Figure 2.2 Laminate with reference axis

There are different types of composite structures. The simplest composite structure is the unidirectional composite in which all fibers run in the same direction parallel to each other in the polymer matrix. Another form of composite structure is the quasi-isotropic composites. Quasi-isotropic means having almost isotropic in plane properties. The most common form of composite is the cross-ply laminate, such as laying up a sequence of unidirectional plies at cross angle. In other structural models such as woven composite, the fibers are braided with each other. This special structure improves the damage tolerance of the composites.

## 2.2 DAMAGE AND FAILURE MECHANISM IN COMPOSITE MATERIALS

### 2.2.1 Damage and Failure due to Mechanical Loading

There are different types of damages in composites under different loading conditions. The first form of damage is the matrix damage which is generally the first mode of damage. Since fibers strength is substantially stronger than the matrix, damage usually appears in the matrix earlier than in the fibers. Matrix cracking is the most general damage mode in composite materials which actually changes the material mechanical properties [28][29]-[36]. Figure 2.3 (a) is an example of fiber matrix debonding and initiation of matrix cracks [34].

Two major types of matrix damages were commonly observed [34]. One form of matrix damage causes more fiber contacts with each other which results in decreasing of electrical impedance. Another form is the damage from cross-ply crack within fiber plies, which results in through-thickness resistance increasing as shown in Figure 2.3 (b). The

third type of damages, as shown in Figure 2.3 (c), is delamination of composites in which the local separation of the fiber plies occurs due to matrix cracking between the layers.

Fiber breakage is another basic types of damage as shown in Figure 2.3 (d). The broken fibers lose their stress carrying capability and transfer load to the unbroken fibers. The discontinuation of electrical conductivity due to the broken fibers results in a general increase of electric resistivity along the fiber direction. Fiber fracture is highly coupled to damage in fiber and matrix materials [37]-[42]. In woven composites, the interaction between fiber and matrix is complicated because the weft and wrap fibers are braided together.

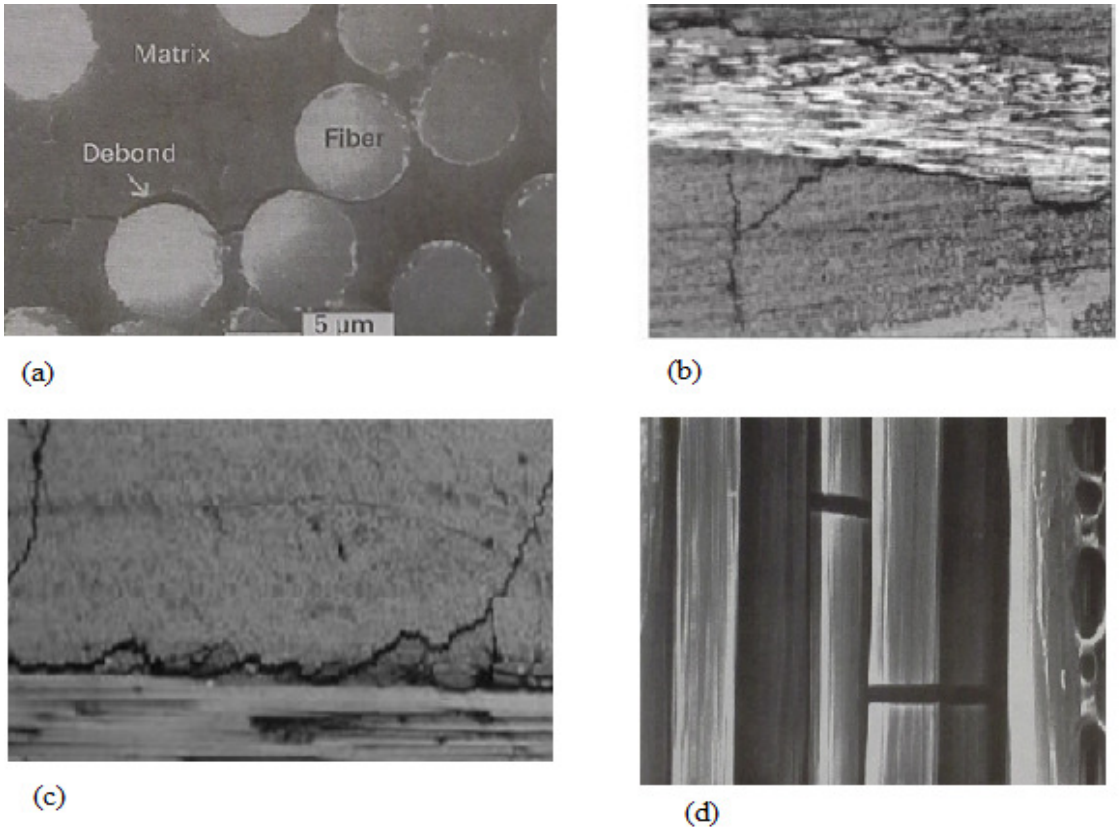


Figure 2.3 Different types of damages (a) matrix crack initiation from fiber/matrix debonding (b) crack within fiber plies (c). Inter-laminar delamination crack of composites (d) fiber break [34]

### 2.2.2 Damage and Failure due to Electric Currents

Composites are somehow electrically conductive because of the electric conductivity of carbon fibers. As fibers are good conductors and can sustain heat generated due to conduction. Most of the damages can be seen in the matrix due to heat generation by Joule effect. Three major types of matrix damages are commonly observed in a lamina plane [19], [20], [28]. One form of matrix damage is due to Joule heating during on axis electrical loading. Due to Joule heating matrix decomposes around the fiber and causes more fiber contacts with each other which results in decreasing of electrical impedance (Figure 2.4(a)). Debonding at the fiber-matrix interface is common damage phenomena due to decompose of matrix. Which can easily explain by thermal-electrical coupling behavior. Another damage form is matrix crack due to electron hopping between two consecutive carbon fiber in a single ply as shown in Figure 2.4 (b). This phenomena is mostly observed during off axis electrical loading. Even during passing current in on axis- direction, current can also flow in off axis direction but different in amount due to anisotropy behavior of composite. In off axis direction there is no direct conduction path so ultimately that leads electron hopping from one fiber to another fiber. During this process it creates a matrix crack between two fibers. The third form of damages can be seen during thickness direction current loading. In thickness direction current causes matrix cracking and/or delamination between the layers interface (Figure 2.4 (c)). There are two reasons for such kind of damages (i) Electron hopping or dielectric breakdown within a lamina between tows or fiber bundles. (ii) Uneven temperature distributions through the thickness [19], [20].

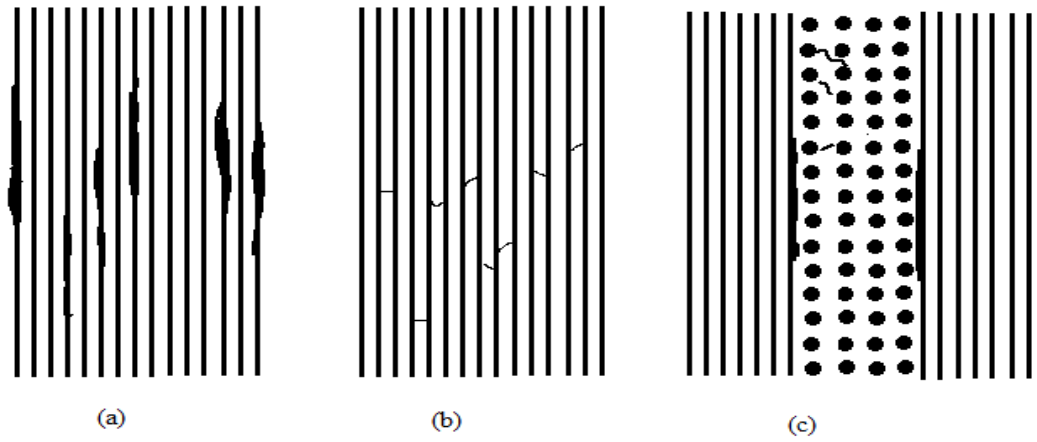


Figure 2.4 Different types of damage due to electric current (a) matrix decomposition and corresponding fiber/matrix debonding. (b) crack within fiber plies. (c) inter-laminar delamination and crack of composites.

## 2.3 CHARACTERIZATION OF MATERIAL STATE

For measuring the change of material state broadband dielectric spectroscopy (BbDS) principle has been used in this research. Broadband dielectric spectroscopy is the interaction of electromagnetic waves with matter in the frequency range from a lower value of $10^{-6}$ Hz to a higher frequency of $10^{12}$ Hz. This dynamic range contains information about the molecular and collective dipolar fluctuation; charge transport and polarization effects occur at inner and outer boundaries in the form of different dielectric properties of the material under study. Figure 2.5 shows the effect of different charge displacement mechanisms on dielectric response and their corresponding effective frequency range.

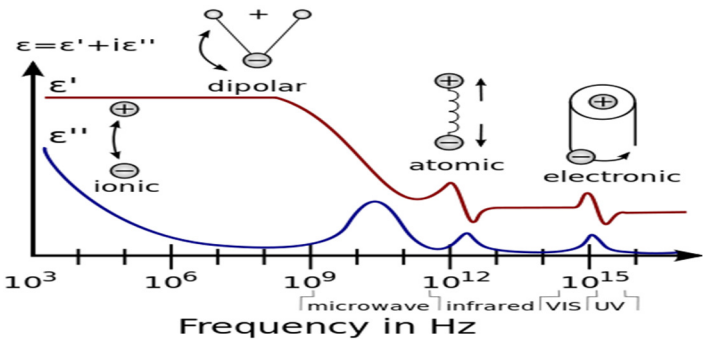


Figure 2.5 Dielectric responses of materials at broad band frequency range [45]

Hence broadband dielectric spectroscopy can be used as a useful tool to obtain a wealth of information on the dynamics of bound dipoles and mobile charge carriers depending on the details of the molecular system and the microstructure in heterogeneous materials. Maxwell's equations describe the interaction between electromagnetic fields and matter [43], [44], [46].

$$\vec{\nabla}.\vec{D}=\rho \tag{2-1}$$

$$\vec{\nabla}\times\vec{H}=\vec{J}+\frac{\partial\vec{D}}{\partial t} \tag{2-2}$$

$$\nabla\times\vec{E}+\frac{\partial\vec{B}}{\partial t}=0 \tag{2-3}$$

$$\vec{\nabla}.\vec{B}=0 \tag{2-4}$$

Here $\vec{D}$ is the dielectric displacement, $\rho$ is the charge density, $\vec{H}$ magnetic field, $\vec{E}$ electric field, $\vec{B}$ magnetic induction and $\vec{J}$ is the current density. In addition to Maxwell's equations, the field must satisfy continuity equations based on the charge density $\rho$ and current density $\vec{J}$ which can be expressed as follows

$$\vec{\nabla}.\vec{J}+\frac{\partial\rho}{\partial t}=0 \tag{2-5}$$

The interrelation between the dielectric displacement $\vec{D}$ and electric field $\vec{E}$ can be expressed by the following equation

$$\vec{D}=\varepsilon_0\vec{E}+\vec{P} \tag{2-6}$$

For a linear relationship between the dielectric displacement $\vec{D}$ and electric field $\vec{E}$ the proportionality constant $\varepsilon$ can be used to express

$$\vec{D} = \varepsilon_r \varepsilon_0 \vec{E} \tag{2-7}$$

Where, $\varepsilon_r$ is the relative permittivity and $\varepsilon_0$ is the permittivity of vacuum. When the polarization $\vec{P}$ , is taken into consideration using equation (2-6) and (2-7)

$$\vec{P} = \chi \varepsilon_0 \vec{E} = \varepsilon_0 \left(\varepsilon_r - 1\right) \vec{E} \tag{2-8}$$

$$\chi = \left(\varepsilon_r - 1\right) \tag{2-9}$$

Here $\chi$ is the polarization coefficient known as the dielectric susceptibility.

Frequency dependent dielectric characteristics (permittivity, impedance, capacity, etc.) under electric field are affected by the heterogeneity of the dielectric medium. For example, the permittivity is influenced by the properties of the constituents, interaction between them and geometrical configuration. This has been used to capture material state change [16]-[20], [40], [41].

# CHAPTER 3
# EXPERIMENTAL PROCEDURE

This thesis explores how electrical current is related to anisotropic material architecture and damage development. Electrical impedance and permittivity measurements are carried out in directions perpendicular, parallel, and at varying angles to the fiber axis. The dependence of the frequency and the temperature upon conductivity has been, likewise, investigated. It is also shown that the high degree of fiber orientation is consistent with the conspicuous anisotropic behavior of the electrical conductivity. Later a damage threshold or damage tolerance approach is presented for measuring durability of woven composite under synergistic mechanical and electrical loading. The microstructure is characterized by 3D X-ray imaging system.

## 3.1 MATERIAL PREPARATION

The specimen is carbon fiber reinforced epoxy polymer. For studying coupled electrical-thermal-mechanical response, unidirectional and quasi-isotropic carbon fiber reinforced epoxy laminate has been chosen. Such laminate architecture provides a heterogeneous material with aligned conductive phase in bulk non-conductive (dielectric) matrix. The surface of this composite sample was first sanded then, silver conductive paste was applied on the surface for reducing contact resistance. The sample size is 25.4x25.4x1.6 mm. Each sample consisted of 8 individual layers. Woven carbon fiber composite has been chosen for damage tolerance and synergistic durability study. Carbon fiber prepreg materials with woven (45/45) fiber pattern and 3900 series thermoset epoxy, was used to make composite

samples. Sample panels with dimensions of 1'x1' were fabricated using a compression molding technique. Each sample panel consisted of 6 layers of the prepreg material. 8 inch long and ¾ inch width specimen coupons were prepared from the sample panel.

A constant pressure of 100 psi was applied during the cure cycle. Heating was adjusted in the compression molding chamber for raising the laminate temperature to $355^0$F at a rate of $3^0$F/min. Then the temperature of laminate was dwelled at $355^0$F for 130 minute. At the end of dwell time, the panel was air cooled from $355^0$ F to room temperature at a rate of $-3^0$ F/min. Figure 3.1 shows the standard cure cycle for preparing the laminate.

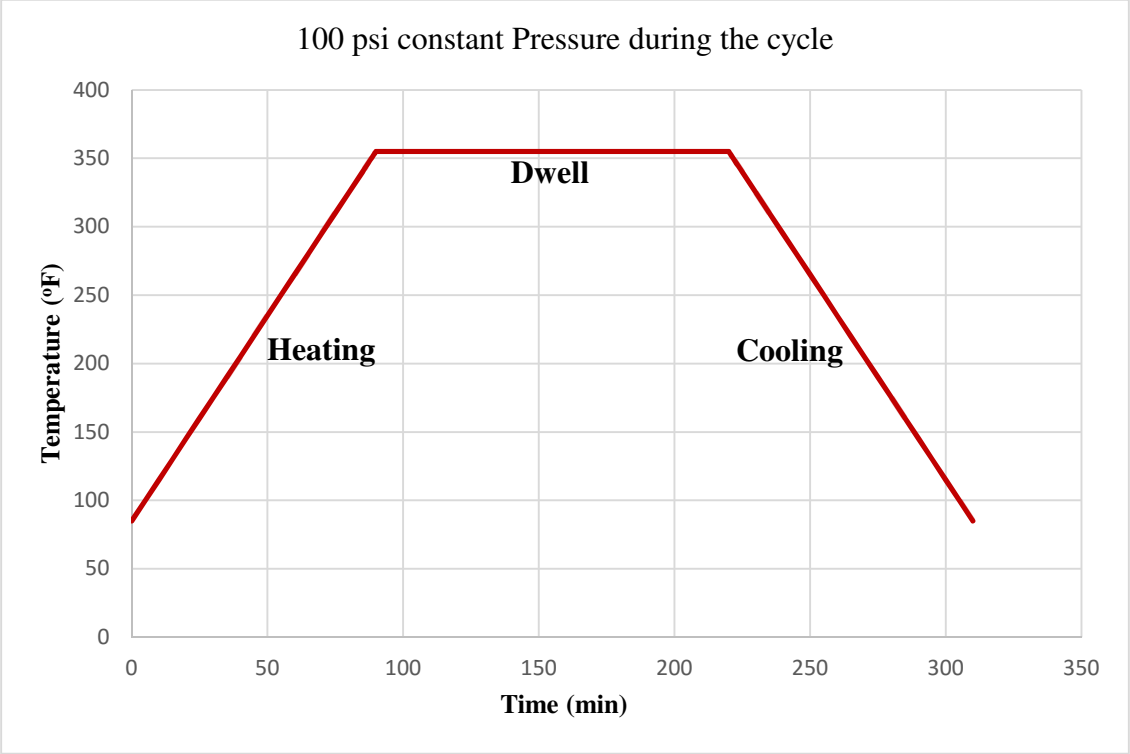


Figure 3.1 Cure cycle for sample panels

### 3.2 EXPERIMENTAL SETUP

The setup is similar to popular broadband dielectric spectroscopy (BbDS) scheme [14]-[18] except the fact that an additional current booster unit is used for varying intensities of

current. Four-probe method is used in this research because the traditional two-probe method is sensitive to the quality of the electrical contacts. In the four-probe method the outer two contacts are for current, and the inner two are for voltage measurement. The four-probe method leaves a lot to be desired because of the high anisotropic properties of carbon fiber composites. In this method the specimen is held between two Cu electrodes which are connected to a BbDS system. For pure BbDS, the test is run in potentiostat mode with a small voltage applied over a wide frequency range ($\mu$ to MHz). For increasing current amplitude, a booster unit is used to provide up to 30 amp current. When it is in operation, the booster unit connects to counter/working electrode while BbDS unit still connects to sensing/reference electrode. A schematic of the test setup is shown in Figure 3.2.

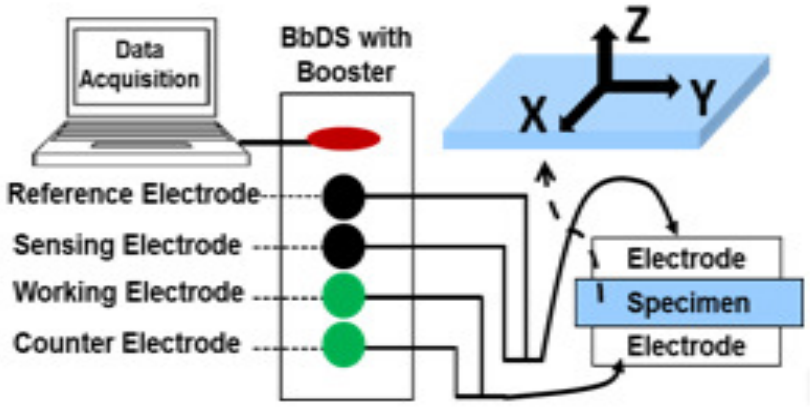


Figure 3.2 Experimental setup of dielectric measurement with varying intensities of electrical current (BbDS with current booster)

For each electrical measurement, a small voltage signal was applied to each specimen, with a frequency sweep ranging from 0.1Hz to 1MHz. The BbDS unit measured the amplitude and phase of the corresponding current. A voltage $U_o$ with a fixed frequency

$\frac{\omega}{2\pi}$ is applied to the sample capacitor. Voltage $U_o$ causes a current $I_o$ at the same frequency in the sample. In addition, there will generally be a phase shift between current and voltage described by the phase angle $\varphi$ shown in Figure 3.3.

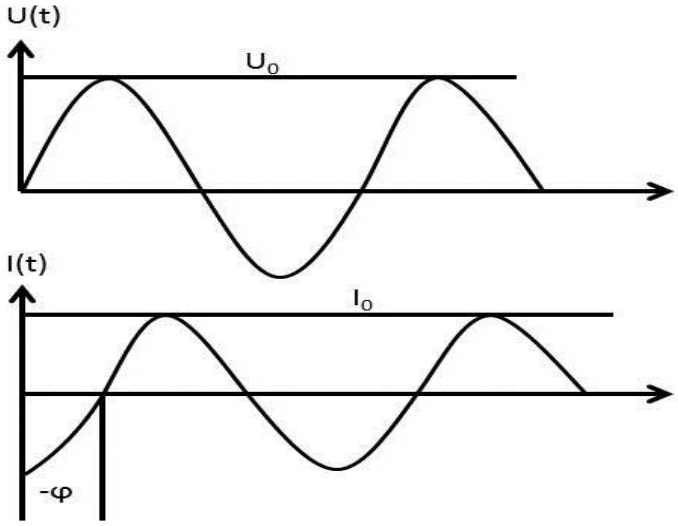


Figure 3.3 Amplitude and phase relations between voltage and current of a sample capacitor for electric measurements.

The ratio between $U_o$ and $I_o$ and the phase angle $\varphi$ are determined by the sample material electrical properties and by the sample geometry. So the appropriate relations in complex notation can be expressed as

$$U(t) = U_0 \cos(\omega t) = Re\left(U^* \exp(i\omega t)\right) \tag{3-1}$$

$$I(t) = I_0 \cos(\omega t + \varphi) = Re\left(I^* \exp(i\omega t)\right) \tag{3-2}$$

With

$$U^* = U_0 \tag{3-3}$$

And

$$I^* = I' + iI'' \tag{3-4}$$

$$I_0 = \sqrt{I'^2 + I''^2} \tag{3-5}$$

$$\tan(\varphi) = \frac{I''}{I'} \tag{3-6}$$

For a sample with linear BbDS response, the measured impedance of the sample capacitor is

$$Z^* = Z' + iZ'' = \frac{U^*}{I^*} \tag{3-7}$$

The complex permittivity can be calculated by

$$\varepsilon^*(\omega) = \varepsilon' - i\varepsilon'' = \frac{-i}{\omega Z^*(\omega)} \cdot \frac{1}{C_0} \tag{3-8}$$

Here $C_0$ is the capacity of the empty sample capacitor.

### 3.3 MECHANICAL RESPONSE MEASUREMENT

The mechanical strength of the coupon samples was measured through a tensile test on a MTS Landmark™ Servo Hydraulic Test System (Figure 3.4). The test was configured to enable measurement of the ultimate breaking load for undamaged and damaged sample. The MTS Landmark™ platform enables the repeatability and the flexibility one needs to perform a full spectrum of static and dynamic material testing.


Figure 3.4 MTS Landmark™ Servohydraulic Test System

## 3.4 IMAGING ANALYSIS

Micro X-ray Computed Tomography (Xradia MicroXCT-400) technology was used to visualize the change of material state (Figure 3.5).

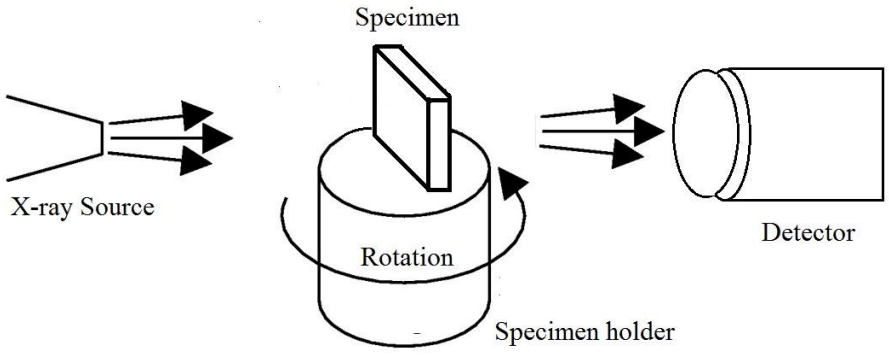


Figure 3.5 Basic principle of Micro-XCT

Basic principle of MicroXCT is shown in Figure 3.5. X-ray computed tomography, uses X-rays to create virtual cross-sections of a physical object; it can be used to recreate

a virtual model (3D model) without destroying the original object. The X-ray source and detector are typically stationary during the scan while the sample rotates. Micro-tomography scanners offers isotropic, or near isotropic, resolution. Display of images does not need to be restricted to the conventional axial images. Instead, it is possible for a software program to build a volume by 'stacking' the individual slices one on top of the other.

## 3.5 THERMOGRAPHIC TEST

Because of the thermal property of the composites, the electrical signal is capable of producing heat in the specimen. The thermal characteristic is observed for both undamaged case and damaged case. An IR camera (FLIR SC6700) was used to capture images of the thermal response of the composites specimen as when the electrical source was applied.

# CHAPTER 4
# RESPONSE OF CARBON FIBER REINFORCED COMPOSITES DUE TO ELECTRICAL CURRENT

BbDS tests are carried out at different current intensities over a wide range of frequencies as well as different intensities of current. For this study, unidirectional and quasi-isotropic carbon fiber reinforced epoxy laminate has been chosen. Such laminate architecture provides a heterogeneous material with aligned conductive phase in bulk non-conductive (dielectric) matrix. This allows a preliminary study of the role of fiber orientation as dominant conductive phase (anisotropic conductivity) and can be insightful for studying other laminates. Fiber orientation angles are varied in unidirectional laminate. For each experiment, electrical current has been applied only in one direction (in-plane x or y and through-thickness, z) of a laminate and corresponding impedance is determined using BbDS setup.

## 4.1 EFFECT OF LAMINATE DESIGN ON ELECTRICAL RESPONSE

Current is applied along x-direction and corresponding impedance is measured over wide frequency range from 1Hz up to 1MHz. The composites are electrically anisotropic. The conduction on different directions within the composite varies with different structures of composites.

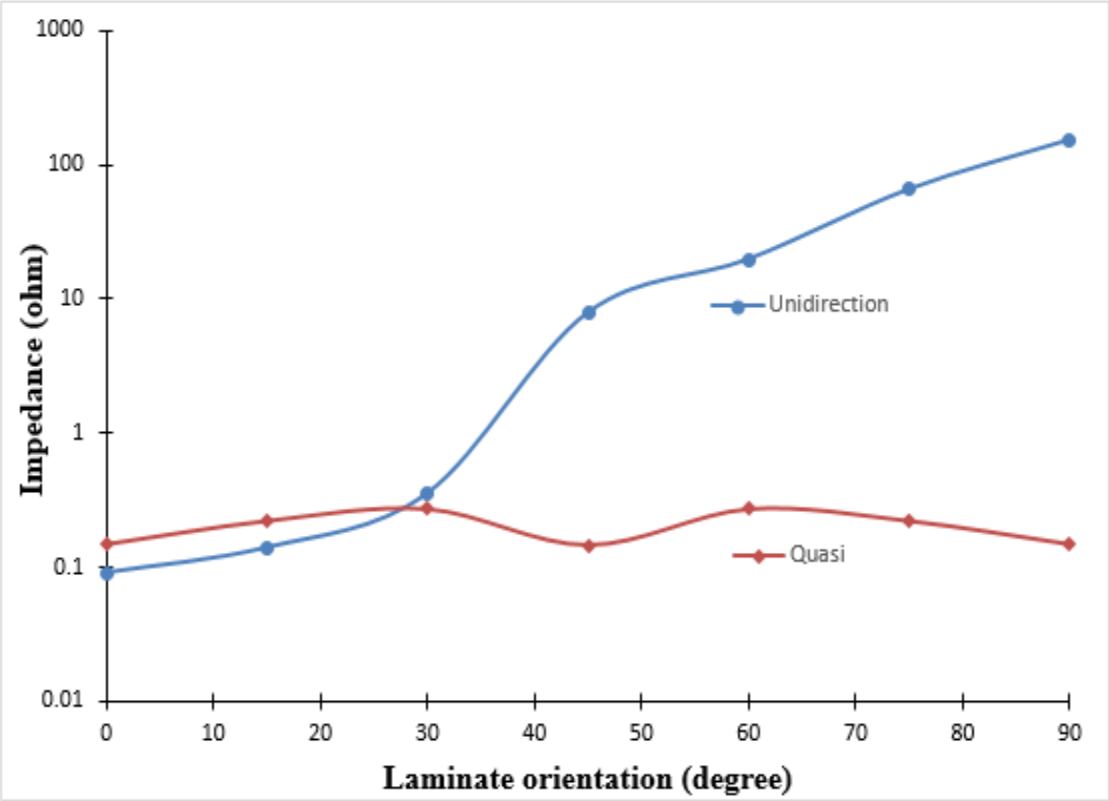


Figure 4.1 Variation of impedance in x-axis of unidirectional laminate and quasi-isotropic laminate with different orientation angle measured by BbDS at 1 kHz.

For unidirectional composites, the impedance in the longitudinal direction is much lower than that in the off-axis direction and maximum in the transverse direction (Figure 4.1). The transverse impedance is 1000 times higher than the fiber direction impedance. In transverse direction electric properties of dielectric matrix and interphase layer are dominant. As a result, laminate shows lower conductivity in transverse direction. Unlike conductivity for unidirectional laminate, the impedance of quasi-isotropic laminate does not increase with laminate orientation angle. This is obvious due to nature of quasi-isotropic $[0/\pm45, 90]_s$ composite. At 0 degree and 45 degree, there is direct conduction path in the x-axis in quasi isotropic composite. Impedance of 0 degree and 45 degree laminates is lower than the 15 and 30 degree oriented quasi-isotropic laminate. Laminate orientation

at 60 and 75 degree has the similar electrical properties of orientation at 15 and 30 degree due to symmetry. Similarly, 0, 45 and 90 degree laminates have similar electrical properties. These base impedance data is representative of the undamaged material state of the composite laminate.

## 4.2 Effect of Increasing Current Intensity in the x-direction of composites Laminate

In the previous section, impedance of undamaged unidirectional laminate (Figure 4.2) at low current intensities was determined. However, in-plane and thickness direction impedance changes with current intensities. Beyond a threshold, there is significant change in impedance which is associated with degradation of the material.

The increasing current intensity (x-direction) causes change in impedance in the fiber direction. As fibers are good conductors and can sustain heat generated due to conduction, there no significant loss of conductivity for 0 degree laminate in the fiber direction up to a threshold value (Figure 4.3). After the threshold value certain damage is observed in the sample which causes change in impedance. That can be captured more clearly by measuring thickness direction impedance while current is passing in x direction. For off axis fiber laminate this threshold limit shifts to the lower current limit as the fibers are oriented away from x axis (Figure 4.3). 3D X-ray imaging confirms the damage state.

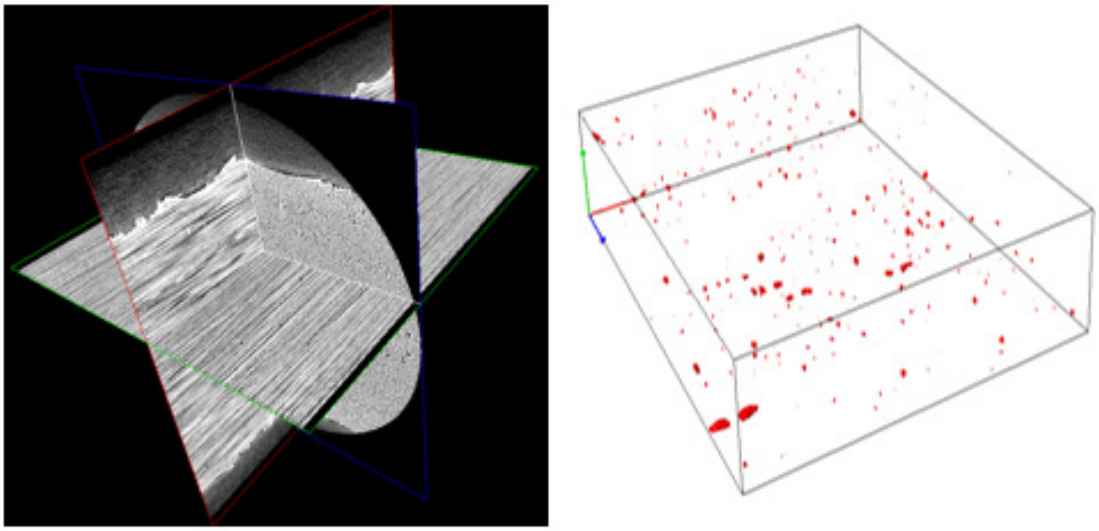

(a) (b)

Figure 4.2 Undamaged sample with manufacturing defects. (a) Planer View (b) 3d View after image processing

To further understand the extent of damage in fiber direction laminates due to increasing current intensities, 3D X-ray microscopic imaging has been done. The imaging system can provide different views of 3D image along with virtual sectioning along different planes. Two major types of matrix damages are commonly observed in a lamina plane. One form of matrix damage is due to Joule heating. Due to Joule heating matrix decomposes around the fiber and causes more fiber contacts with each other which results in decreasing of electrical impedance. Figure 4.5 shows one such example of unidirectional (0 deg) laminate with significant damage after passing 30 A current in fiber (x) direction. The matrix damage cause more fiber contacts with each other which results in decreasing of electrical impedance. Debonding at the fiber-matrix interface is also a common damage phenomenon. The main reason of such kind of damages is also Joule heating, which can be easily explained by thermal-electrical coupling behavior.

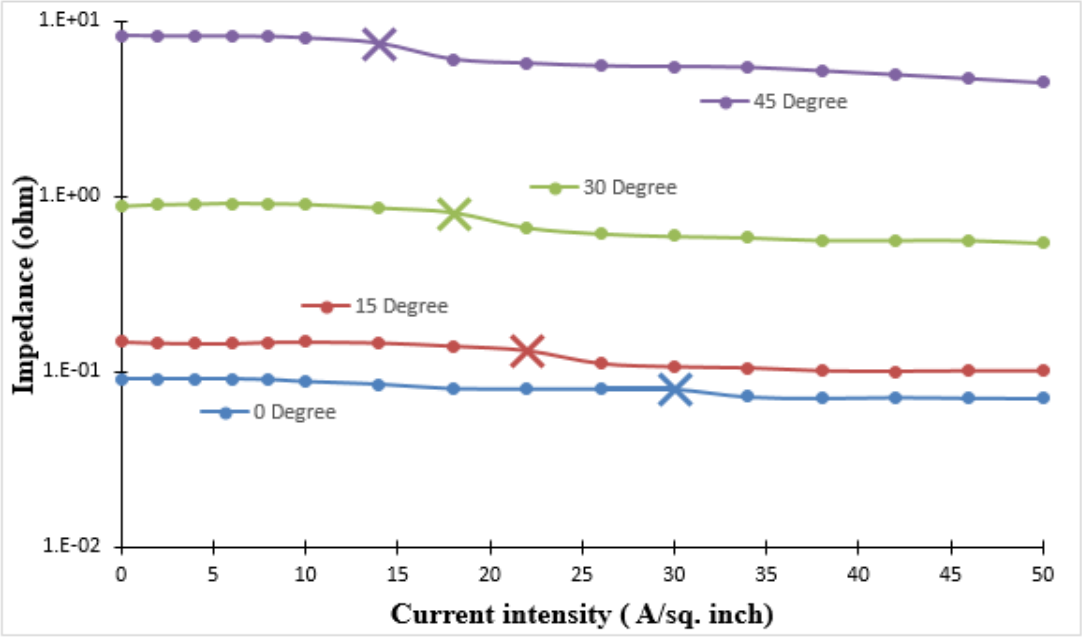


Figure 4.3 Change in x-direction impedance of unidirectional laminate after applying different current intensities in the x-direction (BbDS in Potentiostat mode at 1 kHz)

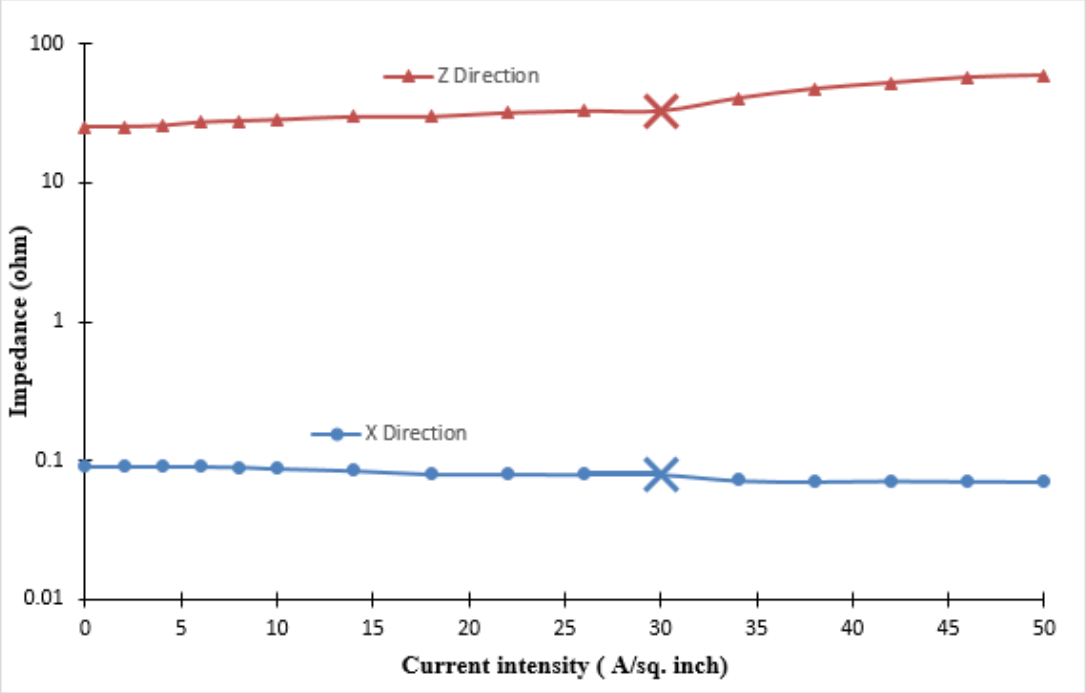


Figure 4.4 Change in x and z direction impedance at of 0-deg laminate measure after applying different current intensities in the x-direction (BbDS in Potentiostat mode at 1 kHz)

Another damage form is matrix cracking. This is due to electron hopping between two consecutive carbon fiber in a single ply. During passing current in x- direction, current also flows in y direction but in different amount due to anisotropy behavior of composite. In y direction there is no direct conduction path so ultimately this leads to electrons hopping from one fiber to another fiber. This process creates a matrix crack between two fibers (Figure 4.5 (a)). These matrix damages result in through-thickness impedance increasing. So if the impedance is investigated as shown in the thickness (z) direction (Figure 4.4) for the same scenario when current is applied in the x-direction, there is significant changes in impedance.

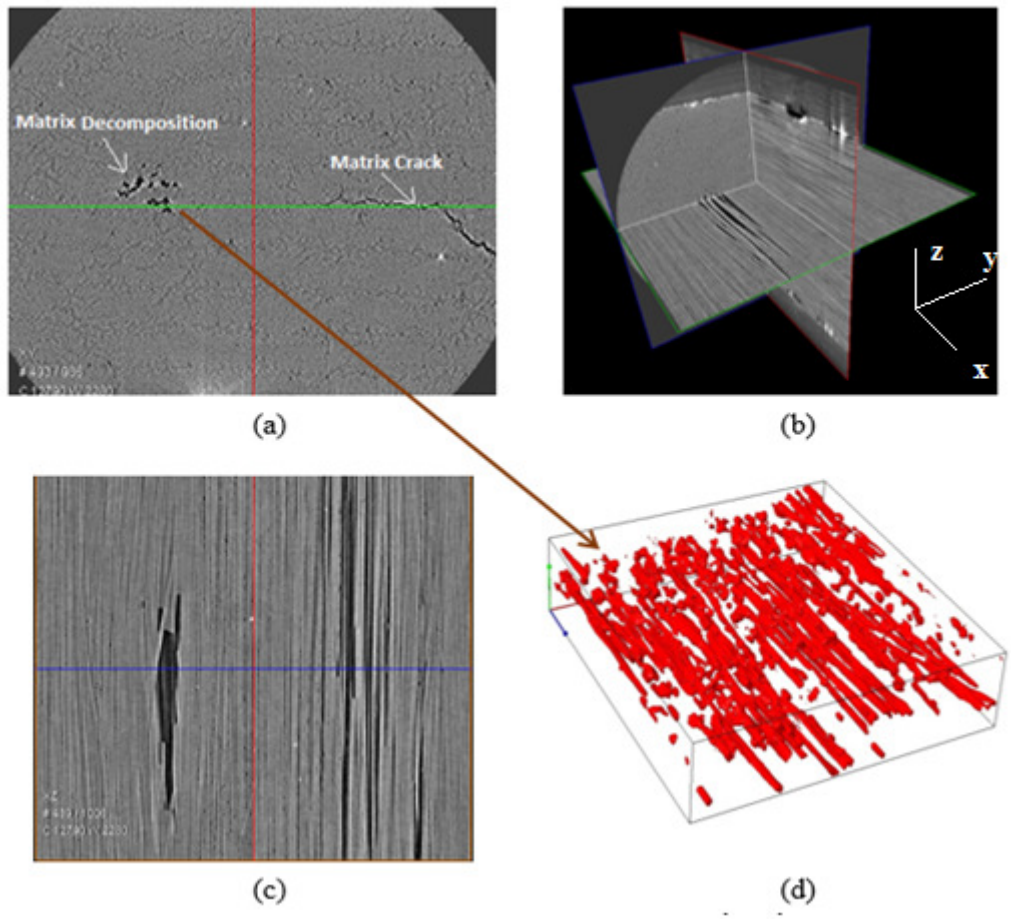


Figure 4.5 Damage due to current in x-direction (a) sectional view (b) planer view (c) in-plane view (d) damage profile

This can be attributed to matrix damage cause by thermal effects due to in-plane (fiber direction) current conduction. The carbon fibers conduct current but generate heat causing matrix damage which cause change in material state. This bulk effect of material state change is captured by the z-direction impedance measurement in the standard BbDS mode. Based on this result of matrix damage due to conduction through fibers, it is expected that fiber orientation will affect z-direction impedance. The main reason of such kind of damages is Joule heating. As presented in earlier data (Figure 4.4), current in the x-direction can cause conductivity change in z-direction also. This significant change in conductivity can be attributed to physical damage of the laminate and the X-ray imaging validates this experimental observation.

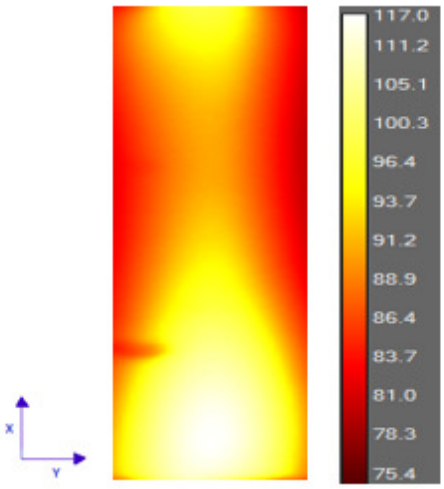


Figure 4.6 Thermal image after passing 20 A/ sq inch current in x-direction

To study thermal behavior associated with conduction of electrical current, the current is applied to the composites sample and corresponding distribution of properties are studied. The change of differential temperature distribution is investigated to explore distribution of damage. The thermal response is studied with thermography tests and results are compared to indicate the damage on the composites using temperature distribution

changes. When the temperature distributions were compared to those of the electrical measurements, they were in good agreement in explaining the potential site of damage. Figure 4.6 shows the thermal distribution due to passing 30 A/ sq inch current in x direction. After passing current in x direction most of the damage is oriented along the fiber as shown in Figure 4.5. That kind of damage pattern is expected as the thermal image from Figure 4.6 shows that thermal conductivity of unidirectional fiber in x direction is dominant than in y and z direction. The main reason of such kind of damage is Joule heating (Equation(4-1)).

$$h = \vec{J}.\vec{E} = \left(\sigma \vec{E}\right).\vec{E} \tag{4-1}$$

Here, $h$ = dissipated heat; $\vec{J}$ = Current Density; $\vec{E}$ = Electrical Field; $\sigma$ =Electrical Conductivity;

As the thermal conductivity is more dominant in x–direction (fiber direction), so damage is also associated with the same direction.

Quasi-isotropic laminates have different fiber orientation at different lamina. Hence they will create a heterogeneous conduction path which will vary from lamina to lamina unlike unidirectional laminate where all lamina had same conduction path (fiber orientation). Extensive damage is observed for a quasi-isotropic laminate as shown in Figure 4.8 after passing 40.0A/sq. inch current in x-direction and corresponding impedance change is showed in Figure 4.7.

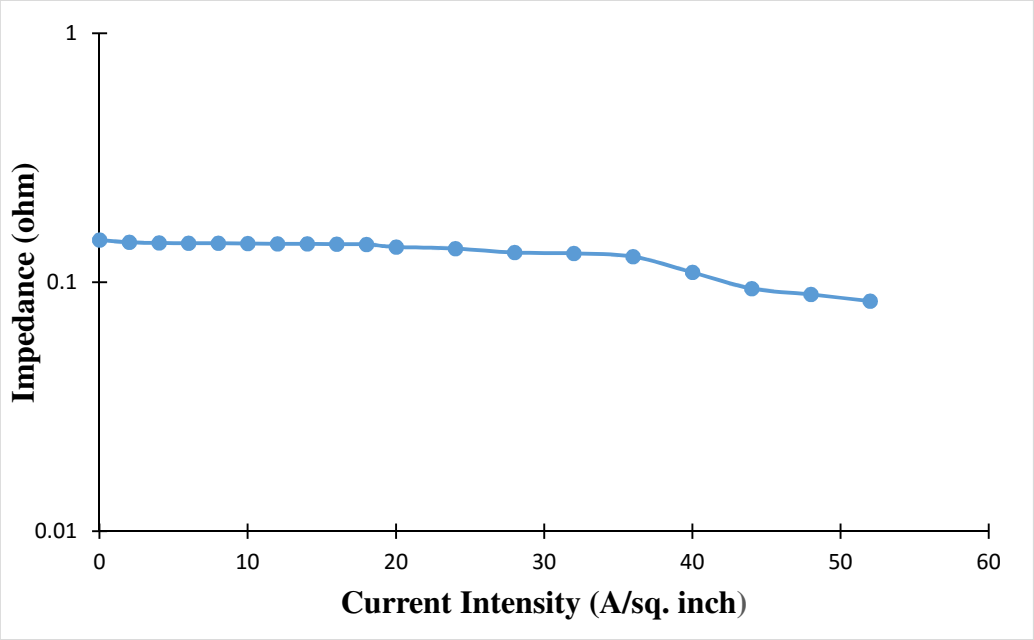


Figure 4.7 Change in x-direction impedance at 1 kHz of quasi-isotropic laminate measure after applying different current intensities in the x-direction

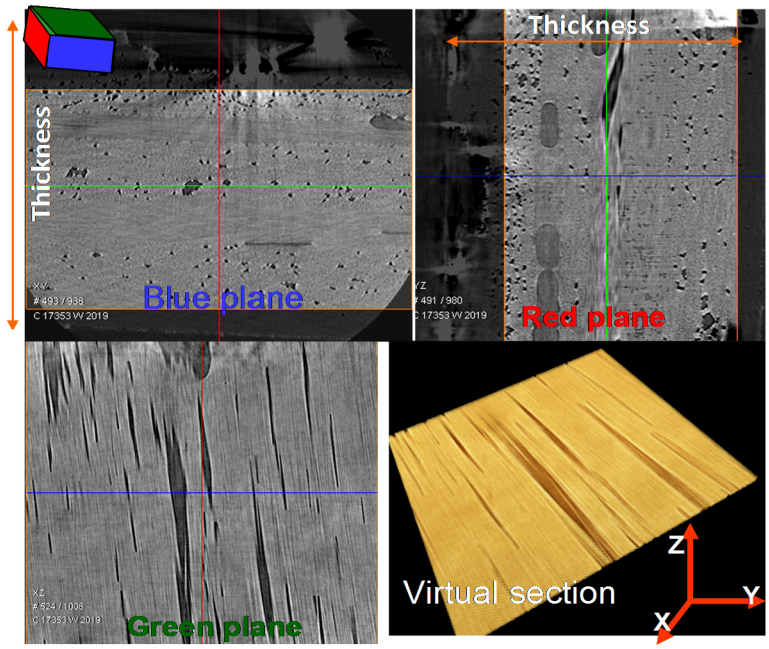


Figure 4.8 Damage in quasi-isotropic composite

Figure 4.9 shows the thermal distribution of a quasi-isotropic composite. The thermal distribution is much more uniform compared to unidirectional composite and it is expected

as the thermal properties of unidirectional composites are dominated by the fiber in the x-direction. So damages are also much more distributed as shown in Figure 4.8

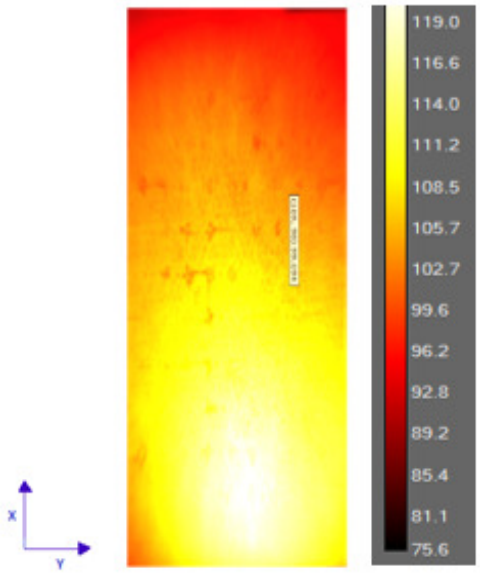


Figure 4.9 Thermal image data after passing 40.0 A/ sq. inch current in x- direction of quasi-isotropic composite laminate

## 4.3 Effect of Increasing Current Intensity in z-direction for Different Unidirectional Laminate Orientation

Current of varying intensities are applied in the z-direction and corresponding impedance is measured. This result is generated for unidirectional laminate of different fiber orientation angles.

For composites, the conductivity in the z direction is dependent on anisotropic nature of laminate. Results of such observations are plotted in the following figures which show threshold values beyond which the impedance significantly changes and this threshold is also different for different laminate orientation (Figure 4.10).

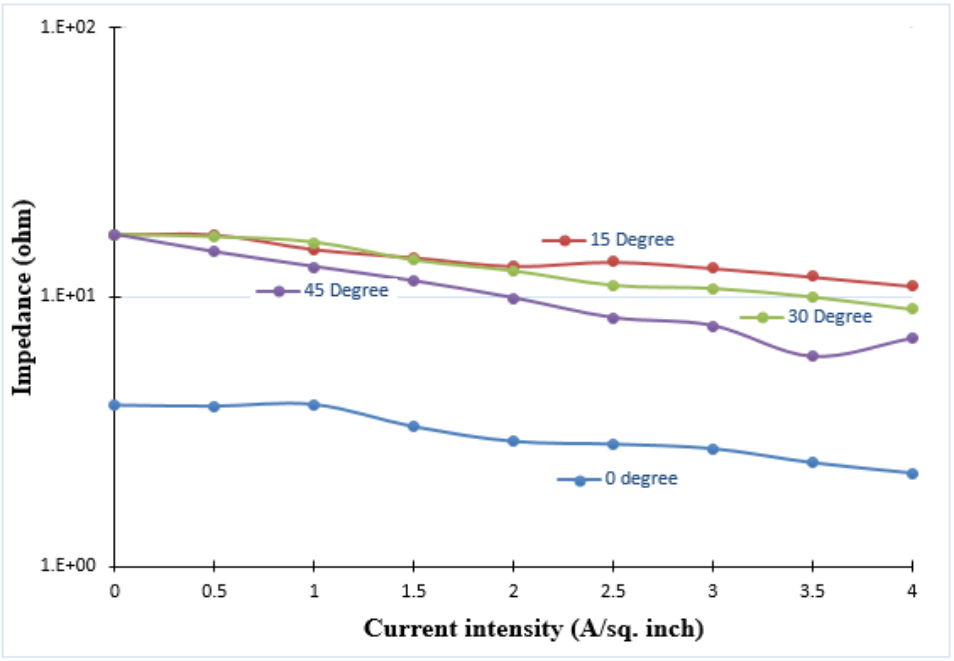


Figure 4.10 Impedance at 1 kHz due to increasing current Intensity in the Z-direction for different orientation

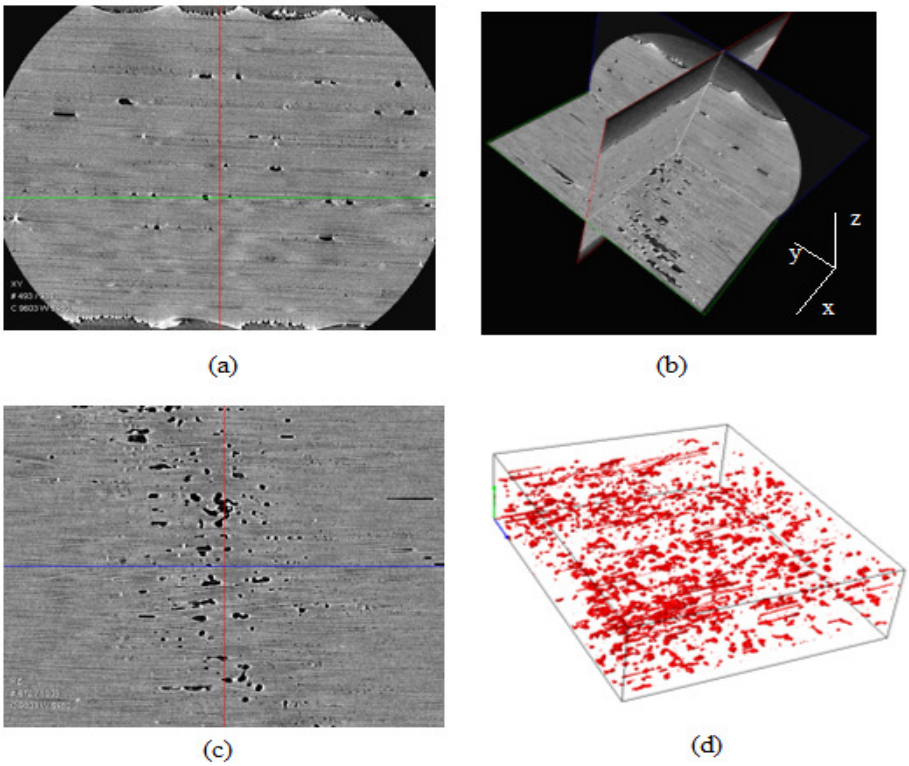


Figure 4.11 Damage due to current in z- direction.(a) sectional View (b) planer view (c) in-plane view (d) damage profile

Figure 4.11 shows unidirectional 0deg laminate with damage due to 2.0A current in z direction. This further validates the observation (Figure 4.11) that at a relatively low intensity of current (2Amp/sq. inch) in the z-direction can cause significant damage in the entire volume of the laminate. Matrix cracking and/or delamination between the layers interface. Electro-thermal response has been discussed further in the subsequent chapters.

Figure 4.12 shows that the thermal distribution after passing 2A/sq inch current in z direction. Most damages can be seen at the interface between two lamina. There are two reasons for such kind of damage pattern (i) electron hopping or dielectric breakdown between two laminae (ii) uneven temperature distributions through the thickness. It is believed to be due to the fact that the laminate has more conductive heterogeneity in the thickness direction leading to more non-uniform heat dissipation.

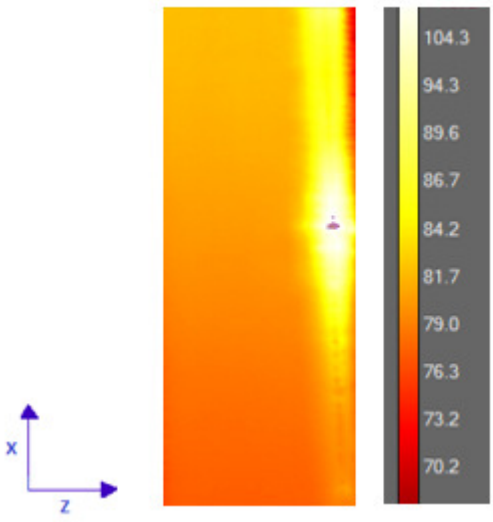


Figure 4.12 Thermal Image After Passing 2.0 A/Sq Inch Current In z-direction

# CHAPTER 5
# EFFECT OF ELECTRICAL CURRENT ON EXISTING DAMAGE AND LOSS OF MECHANICAL PROPERTIES OF WOVEN CARBON FIBER COMPOSITE MATERIALS

Traditionally, investigators have focused on mechanical durability and damage tolerance [30], [47], [48], [49]. In that work, evolution of damage and loss of mechanical properties (such as strength and stiffness) have been studied extensively. For example, Reifsnider's group have done pioneering work to show how evolving damage subsequently controls the life of a composite materials [30], [48]. However, electrical behaviors of composite materials have not been studied in greater details from this durability perspective. Specifically, it is not well understood how existing mechanical damage may influence subsequent electrical behavior and it is also unknown how application of electrical current will change mechanical strength. In this chapter, results from an exploratory work will be presented on this topic. These should be considered very preliminary work and surely needs further studies in the future.

Carbon fiber prepreg materials with woven (45/45) fiber pattern and 3900 series thermoset epoxy, was used to make composite samples. Sample panels with dimensions of 1'x1' were fabricated using a compression molding technique. Each sample panel consisted of 6 layers of the prepreg material. 8 inch long and ¾ inch width specimen coupons were prepared from the sample panels.

## 5.1 EFFECT OF ELECTRICAL CURRENT ON REMAINING TENSILE STRENGTH OF WOVEN COMPOSITE MATERIALS

As discussed in earlier chapters, there is significant change in electrical properties beyond a threshold, this is associated with degradation of the material. Hence this material state (microstructure) change with increasing current intensities is expected to affect mechanical properties also.

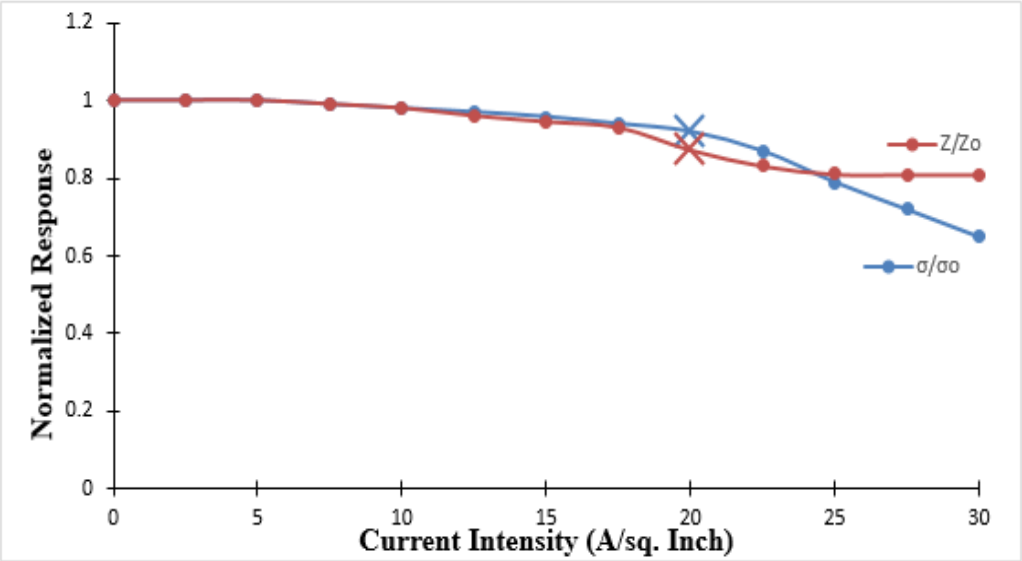


Figure 5.1 Normalize response of mechanical strength and impedance at 1 kHz with current intensity

( $\sigma$ = strength at different current intensity, $\sigma_o$ = strength of undamaged sample, $Z$ = impedance at different current intensity, $Z_o$ = impedance of undamaged sample)

In this experiment, increasing intensities of current has been applied and at each intensity level mechanical strength test has been performed. After the threshold value certain damage is observed in the sample which causes change in impedance. After this threshold value there is a change in mechanical strength also. As fibers are good conductors

and can sustain heat generated due to conduction, there no significant loss of mechanical properties to a threshold value (Figure 5.1). Later 3D X-ray imaging confirms the damage state. This confirms that mechanical durability changes with electrical current. If the electrical current exceeds the threshold limit, it may cause or accelerate subsequent failure due to mechanical loading.

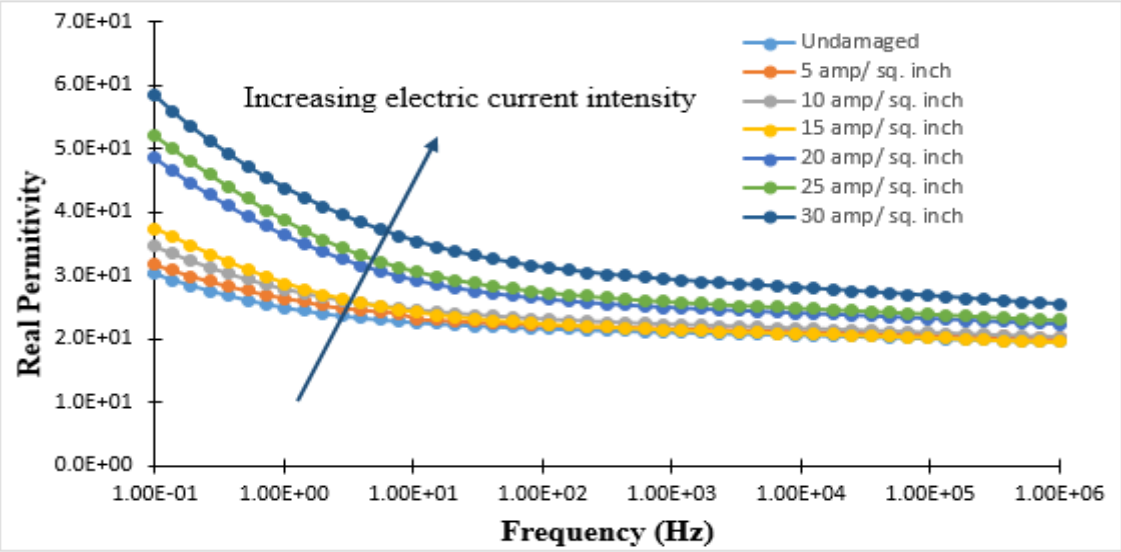


Figure 5.2 Variation of real permittivity of composite with current intensity

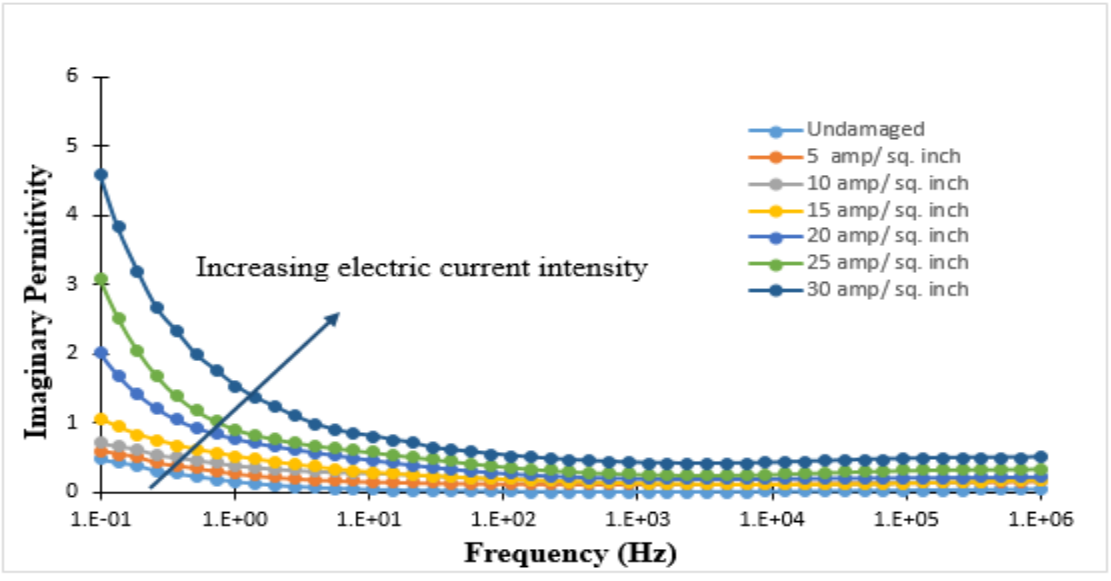


Figure 5.3 Imaginary permittivity of composite with current intensity

Earlier work by Reifsnider and Majumdar group have shown that material state change can be captured in terms of different state variables such as permittivity which is influenced by the properties of the constituents, interaction between them and geometrical configuration [18]-[20], [40], [41]. Figure 5.2 and Figure 5.3 show how real permittivity and imaginary permittivity change with applied current which can give the description of the material state. Initial increasing permittivity confirms the initial damage growth and, after a certain threshold (15-20 Amp/sq inch), there is significant change in permittivity which confirms the corresponding property loss.

To further understand the extent of damage in x direction laminates due to increasing current intensities, 3D x-ray microscopic imaging has been done. The imaging system can provide different views of 3D image along with virtual sectioning along different planes. Major types of matrix damage are commonly observed in a lamina plane and that is due to Joule heating. Due to Joule heating matrix decomposes around the fiber and causes more fiber contacts with each other, results in decreasing of electrical impedance (Figure 5.1). Figure 5.4 show one such example of woven laminate with significant damage after passing 30.0A/sq. inch current in x direction. The thermal response is studied with thermography tests and results are compared to indicate the damage on the composite using temperature distribution changes. The fibers are oriented (+45/-45) direction the temperature along that direction is much higher. Figure 5.4 shows that all the damages are associated around the fiber direction, the temperature distribution confirms such damage behavior.

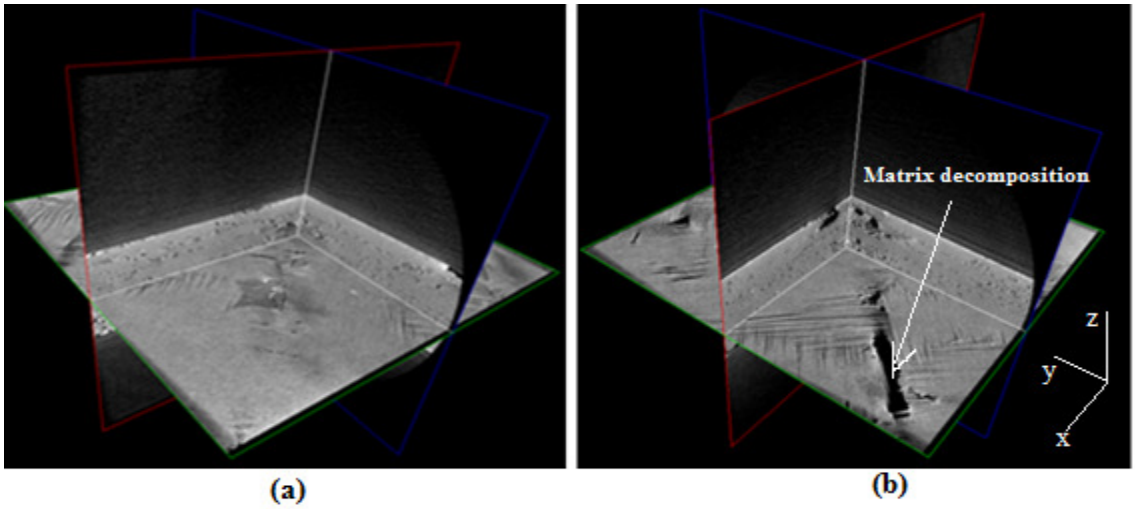


Figure 5.4 3D x-ray image of undamaged and damaged composite sample (a) planer view of undamaged sample (b) planer view of damaged sample (30 A/sq. inch)

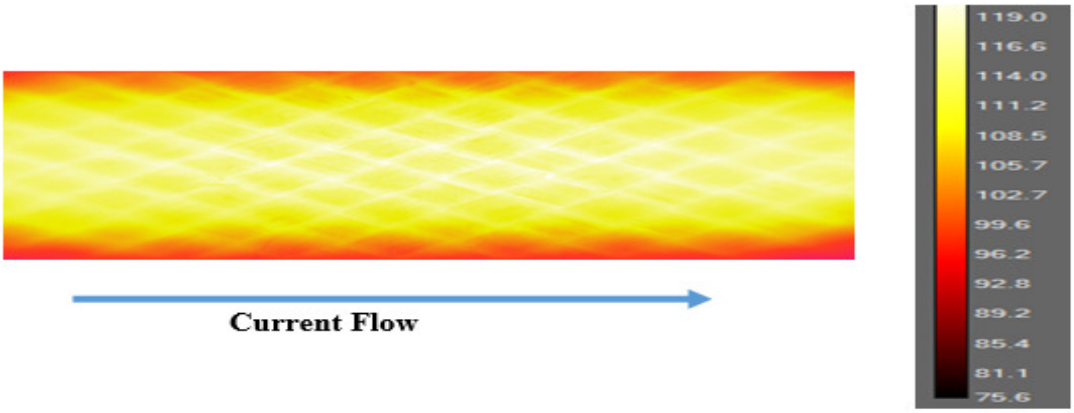


Figure 5.5 Temperature distribution after passing 30A/ sq. inch current to x direction

## 5.2 Effect of Existing damage and Increasing current intensity on remaining tensile Strength of woven composites

In previous section evolution of strength of composite material and damage with electric current has been discussed. But electric loads are not always exposed to initial material state. Composite structures are subjected to different kinds of mechanical loads during their service life. Due to mechanical load, there is a chance of changing material state and subsequently electrical load may causes serious change in material state and reduce the

service life of structure. In this study, impact load (4J, BVD) was applied to initiate mechanical damage to the material. Then electric current study was carried out and remaining mechanical strength was measured at every current value.

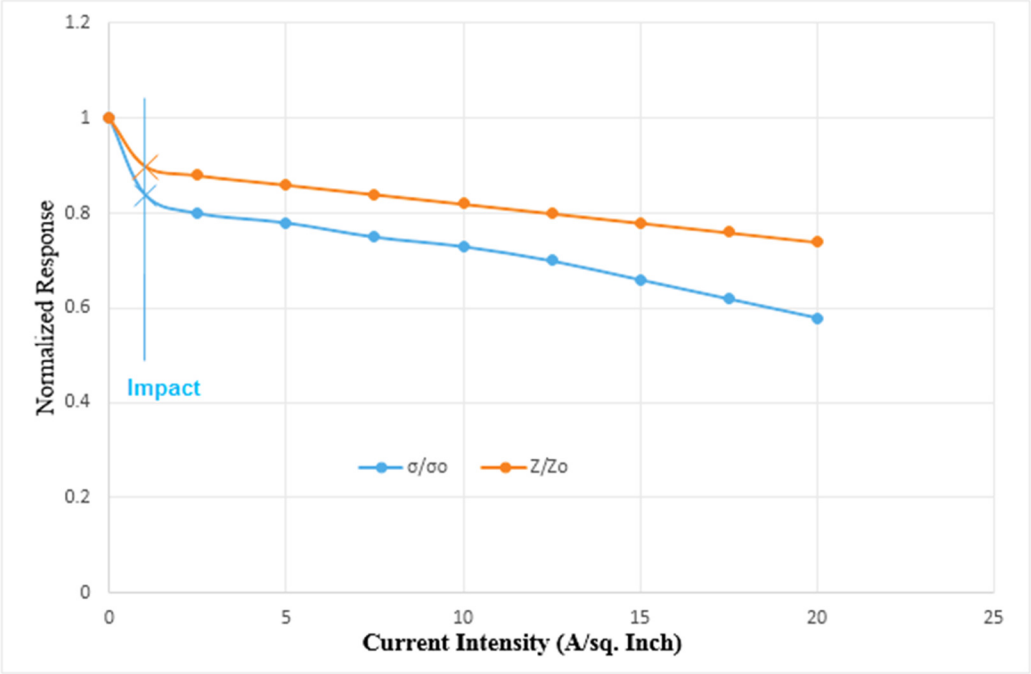


Figure 5.6 Normalize response of mechanical strength and impedance due to electric current with prior damage.

Like pure electrical loading this study doesn't show any threshold value rather prior damage due to impact has a gradual effect on mechanical strength and electrical properties. Figure 5.6 shows the change of mechanical strength and electrical properties due to impact and then gradual electric current. Mechanical strength is dropped around 20% due to mechanical impact damage and then gradually dropped up to 60% at 20A/ sq. inch electric current. Figure 5.7 and Figure 5.8 show how real permittivity and imaginary permittivity change with applied current which can give the description of material state. Permittivity is increased suddenly due to prior mechanical damage and later increased gradually with current intensity. This confirms growth of prior damage with increasing current.

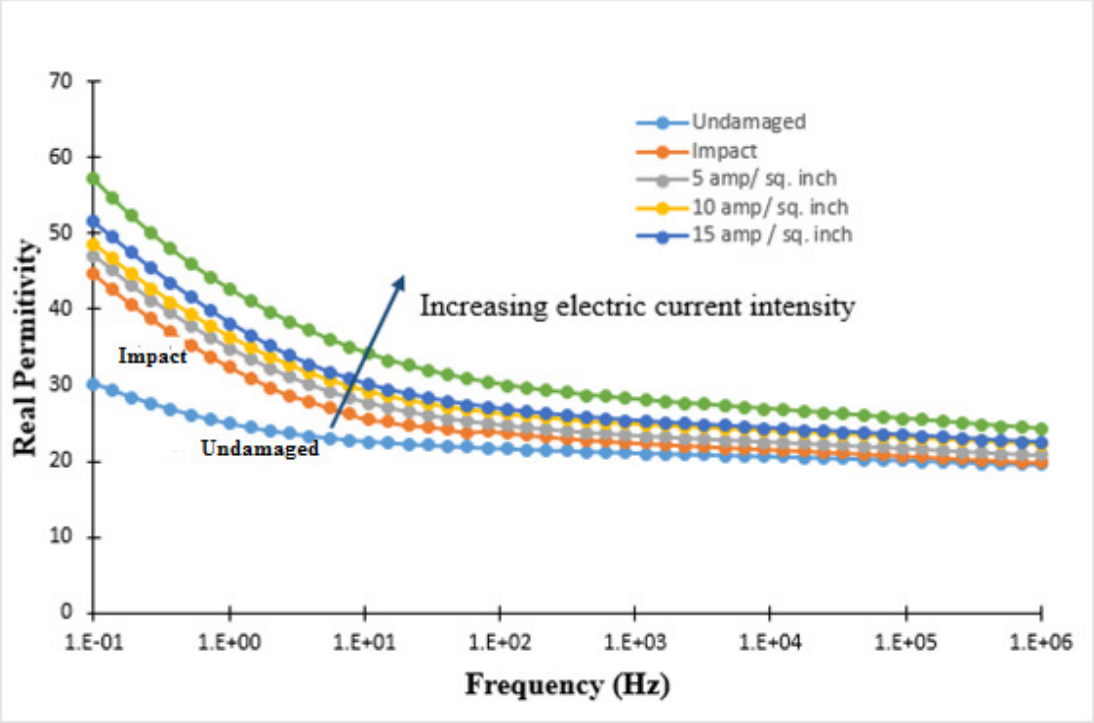


Figure 5.7 Change of real permittivity of composite due to electric current with prior damage

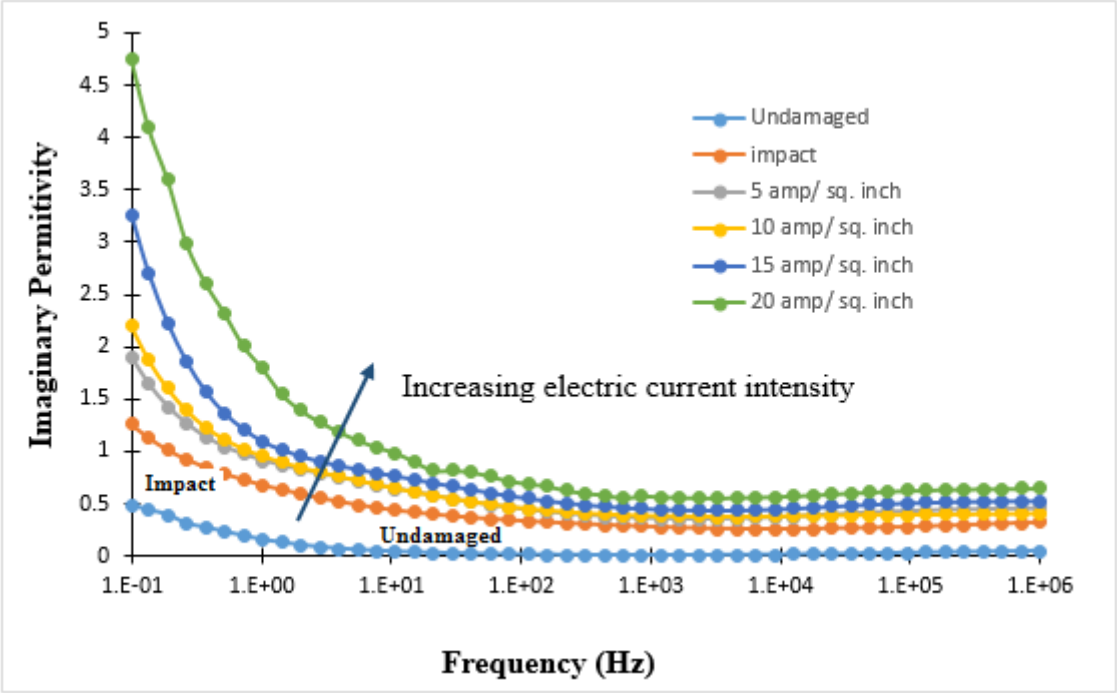


Figure 5.8 Change of imaginary permittivity of composite due to electric current with prior damage

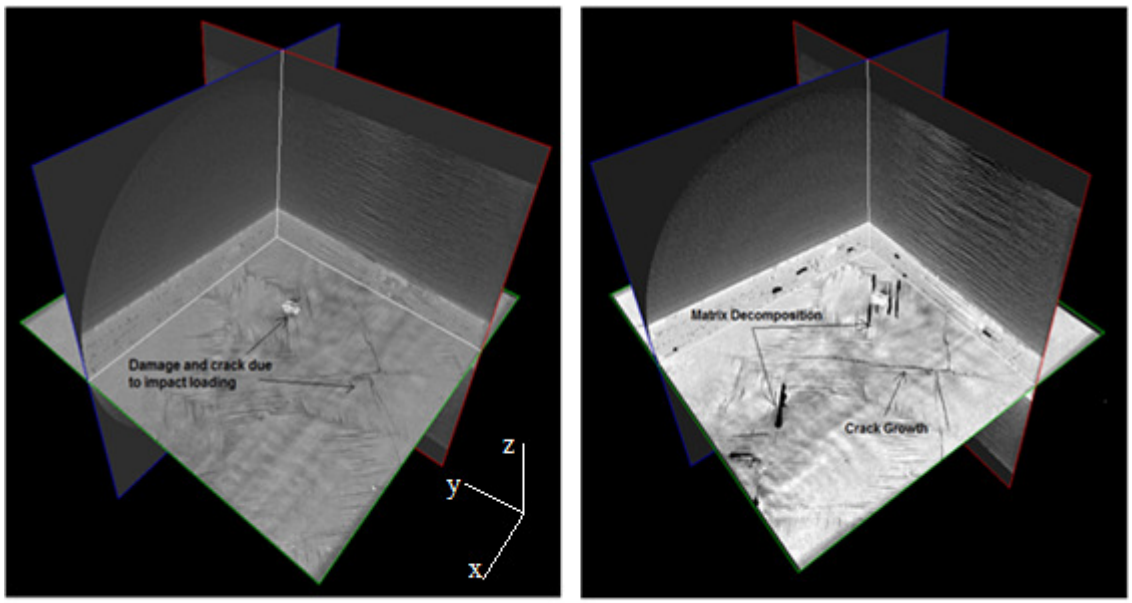


Figure 5.9 Evolution of damage due to electric current with prior mechanical damage (a) damage due to impact (b) damage due to electric cuurent with prior mechanical damage

The damage phenomena are different due to prior mechanical damage than pure electrical loading damage. Prior mechanical damage has great influence on the subsequent electrical damage. There are two types of mechanical damage that were observed after impact loading. One kind of damage around the fiber or fiber matrix debonding; and other one is cracking in the matrix (Figure 5.9 (a)). Damaged around the fiber causes more fiber contacts with each other which results in decreasing electrical impedance which ultimately leads a biased path for electric current. More Joule heating was observed around that area and causes significant damage (Figure 5.9 (b)). Matrix crack makes the material weak in terms of dielectric breakdown strength. So electron hopping or jumping are common phenomena into the prior crack path which ultimately causes crack growth (Figure 5.9 (b)).

# CHAPTER 6
# FINITE ELEMENT ANALYSIS OF ELECTRO-THERMAL RESPONSE DUE TO DEGRADED MICROSTRUCTURE OF COMPOSITE MATERIALS

To conduct the coupled electro-thermal analysis, Joule heating due to electric current was considered for numerical studies. In numerical study, the change of differential electrical potential is investigated to effect of the damage and to correlate with the distribution of damage. This study is very important to observe how damage can change the electric potential, current density, and thermal distribution over the evolving or degrading microstructure. There is not such analysis has been reported in the literature and this is a unique contribution.

## 6.1 METHODOLOGY

The objectives of the modeling section in this research are to simulate the electrical potential distribution and thermal distribution for undamaged and damaged composite materials. The corresponding impedance values are also measured to correlate the change of material state. Electrical properties are coupled with damage state so change of material state ultimately causes change in potential distribution, current density, and temperature distribution. The following equations are used for the coupled thermal-electrical study and a commercial code COMSOL has been used for solution.

Governing equation

$$\vec{\nabla}.\vec{J} = Q_j \tag{6-1}$$

$$\vec{J} = \sigma \vec{E} \tag{6-2}$$

$$\vec{E} = -\nabla \vec{V} \tag{6-3}$$

$$\vec{D} = \varepsilon_r \varepsilon_o \vec{E} \tag{6-4}$$

Boundary condition on insulated surface

$$\vec{n}.\vec{J} = 0 \tag{6-5}$$

$$\vec{V} = 0 \tag{6-6}$$

Electrical-thermal coupling

$$h = \vec{J}.\vec{E} = (\sigma \vec{E}).\vec{E} \tag{6-7}$$

Here, $\vec{J}$ =current density, $\vec{E}$ =electric field, $V$ =Electric potential, $\sigma$ =electrical conductivity, $h$=heat due to Joule heating, $\varepsilon_r$ =relative permittivity, $\varepsilon_0$ = vacuum permittivity, $D$ = dielectric displacement

For impedance measurement, the following equations are used.

Governing equations

$$\vec{D} = \varepsilon_o \varepsilon_r \vec{E} \tag{6-8}$$

$$\vec{\nabla}.\vec{D} = \rho \tag{6-9}$$

Here, $\rho$ is the charge density. From Maxwell's law the following equations can be written

$$\vec{\nabla}.\vec{J} = -\frac{d\rho}{dt} \tag{6-10}$$

From Ohm's law

$$\vec{J} = \sigma \vec{E} \tag{6-11}$$

From above equations the following equation can be written

$$\vec{\nabla}.\left(\vec{J}+\frac{d\vec{D}}{dt}\right)=0 \tag{6-12}$$

Using equation (6-8) and (6-11), we get

$$\vec{\nabla}.\left(\sigma\vec{E}+\frac{d(\varepsilon_o\varepsilon_r\vec{E})}{dt}\right)=0 \tag{6-13}$$

In case of sinusoidal electric field $\vec{E}$ of angular frequency $\omega$

$$\vec{\nabla}.\left(\sigma+i\omega\varepsilon_o\varepsilon_r\right)\vec{E}=0 \tag{6-14}$$

$$\vec{E}=-\vec{\nabla}V \tag{6-15}$$

The following equation can be written

$$\vec{\nabla}.[\left(\sigma+i\omega\varepsilon_o\varepsilon_r\right)\vec{\nabla}V]=0 \tag{6-16}$$

From above equation, it can be seen that, in a heterogeneous material, the product of the physical properties (some form of the conductivity and permittivity) and the slope of the potential must be a constant as it crosses material boundaries. The interacting field is a result of the charge difference at the interface and, unless the conductivity and permittivity of adjacent material phases are identical, there is a disruption of charge transfer at the material boundary which results in internal polarization.

Boundary Conditions:

Potential on the one side of sample is

$$V=U=U_o e^{-i\omega t} \tag{6-17}$$

Potential on the other side of the sample is

$$V = 0 \tag{6-18}$$

Boundary conditions on the interfaces are

$$V_1 = V_2 \tag{6-19}$$

$$\varepsilon_1 \hat{n}.\nabla V_1 = \varepsilon_2 \hat{n}.\nabla V_2 \tag{6-20}$$

here $\hat{n}$ is the normal unit vector.

Boundary condition on insulated surface is

$$\hat{n}.\vec{\nabla} V = 0 \tag{6-21}$$

Here $\hat{n}$ is the normal unit vector to the side plane.

## 6.2 ELECTRO-THERMAL RESPONSE ON EVOLVING MATERIAL STATE

The coupled thermal-electrical element model has been developed to analyze a real composite structure (Figure 6.1). The main advantage of taking a real structure image as finite element analysis (FEA) input is that it considers the actual distribution of the material damage. After image processing the real structure with damage has been taken as FEA input. The material properties are assumed as homogenous except in damage area. Heterogeneity comes due to damage in the sample. Maxwell's equation is solved to find out the current density and potential distribution over the volume. Electrical-thermal coupling equation is used to couple the thermal problem with electrical problem. The electrical potential distribution on the composite specimen can be simulated by FEA with applying a current load and boundary conditions.

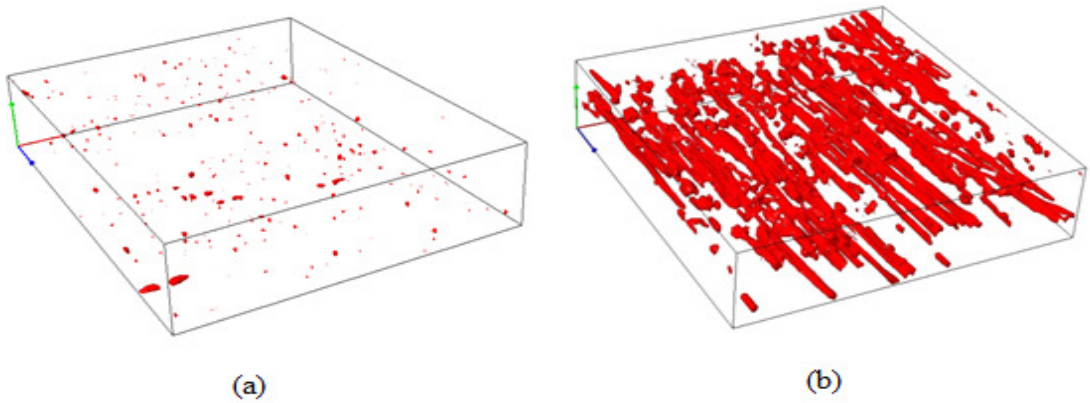


Figure 6.1 Real composite structure for Multiphysics modeling (a) Undamaged with manufacturing defect (b) Damaged after 30 A/sq. inch current intensity

For predicting the electrical response, the entire volume is presented as homogenous medium and damages have different material properties than the homogenous medium. The goal is to investigate the thermal-electrical response with material damage state. The material properties are taken from the experimental study. The FEA model, which simplifies the complicated experimental procedure, is capable of conducting convenient studies without any troublesome effect that is accompanied to the experiment. For example, electric loading during the experiment might have defect, as the electrodes are handmade and hard to be perfectly attached to the surface to conduct the loads. Any mismatch between the sample and electrode causes contact resistance, and any kind of contact resistance is responsible for heating source. This thermal-electrical FEA model provides full control on the loading sections. The role of contact resistance either can be compensated for or included in the model if the electrode is included in the FE model.

### 6.2.1 Electric Potential Distribution

The electric potential (voltage) at any volume is produced by a continuous distribution of charge. Figure 6.2 and Figure 6.3 shows the electric potential distribution of undamaged and damaged composite structure. The electrical potential reaches the highest value at the loading

side and gradually decreases. Corresponding to the composite specimen for electrical current experiment, the load applied in this model is equivalent to 2A/ sq. inch current for undamaged sample and 30A/ sq. inch for damaged sample. As shown in Figure 6.3, the electrical potential distribution changes with the damage around the damage region. It can be seen that the potential distribution of undamaged and damaged sample reflect the damage effects of the electrical potential on the composite. The electrical current goes to an alternative route when damage occurs, which leads to the changes of electrical potential around the damage.

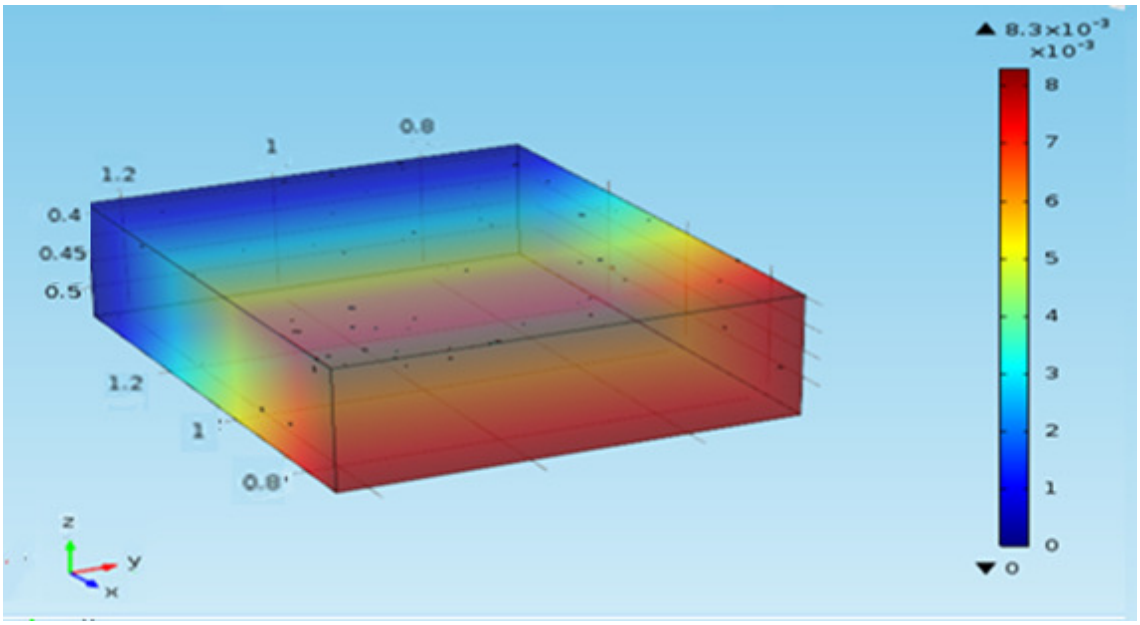


Figure 6.2 Potential distribution on undamaged sample after passing 2A/sq inch current in x- direction

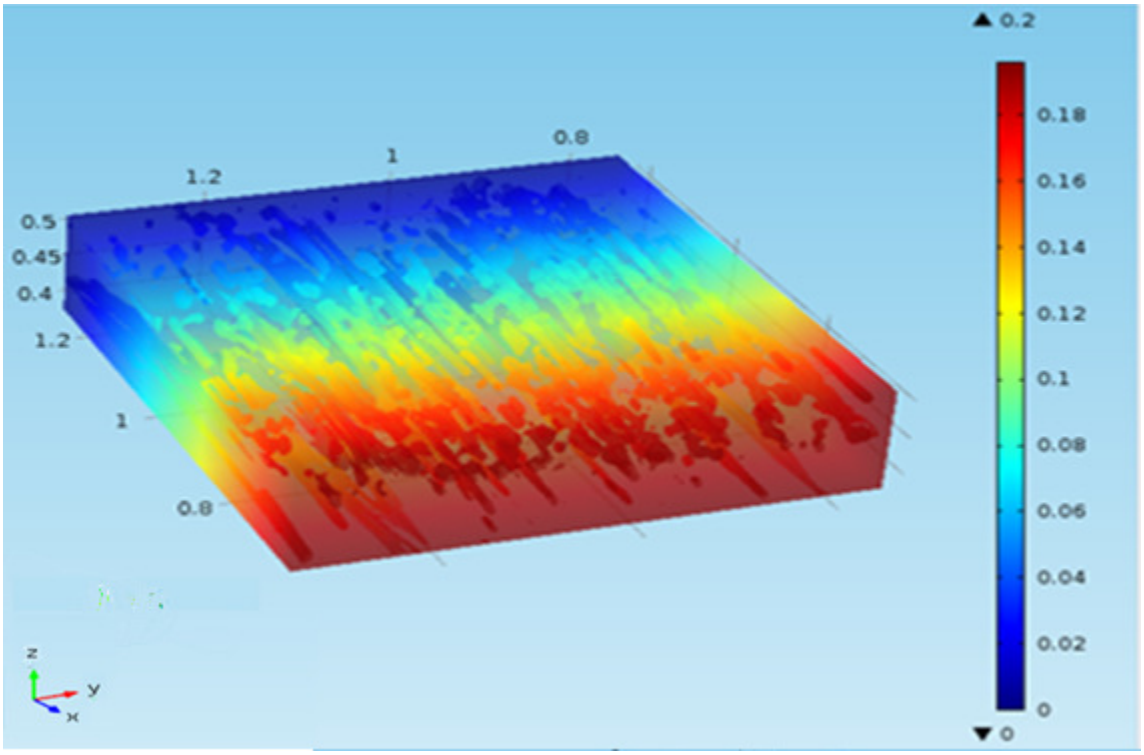


Figure 6.3 Potential distribution on damaged sample after passing 30A/sq inch current in x- direction

Figure 6.4 shows the corresponding impedance value of undamaged and damaged sample. The impedance value is higher for damages sample than undamaged one. Damaged sample contains damage area with homogenous medium surrounding to it and presence of damage causes loss of conductivity. In contrast during the experiment damages due to current causes fiber to fiber contact and ultimately reduce the impedance.

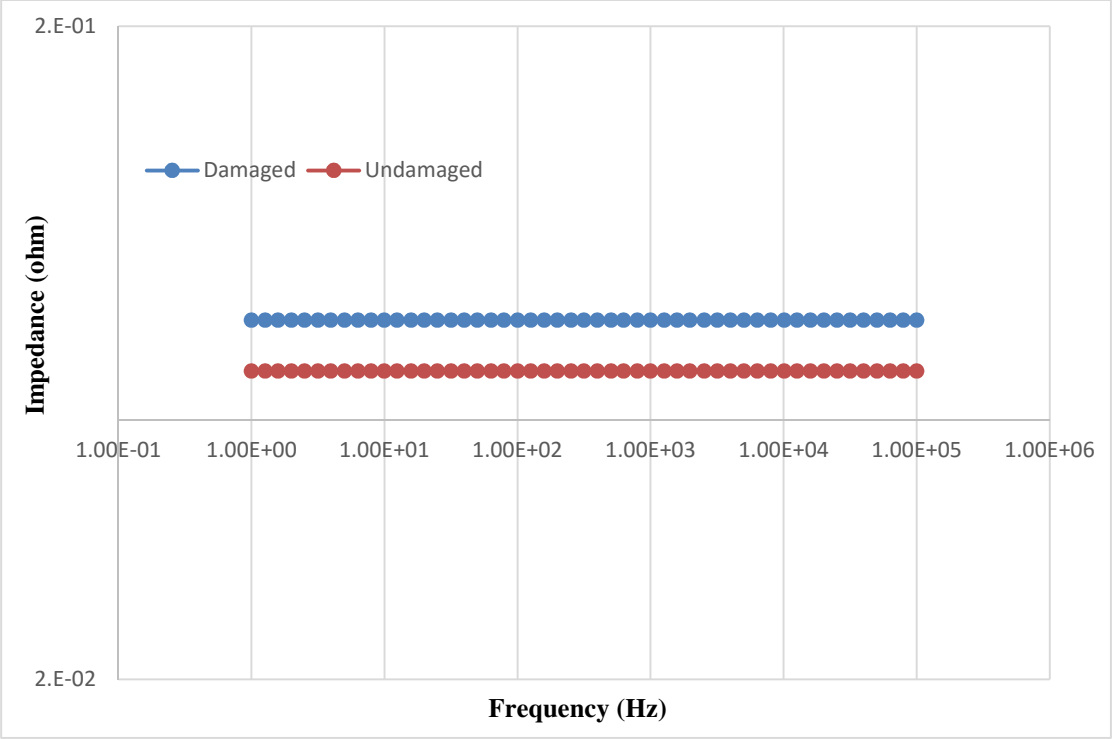


Figure 6.4 Impedance of undamaged and damaged sample

### 6.2.2 Electric current density

Electric current density over the surface is very important. Electric current density heavily depends on conductivity. Heterogeneous conductivity causes change in electric current density. Damage in the homogenous medium can causes heterogeneous conductivity. Electric current density arises from the charge flow and thus it depends on the conductivity of the sample.

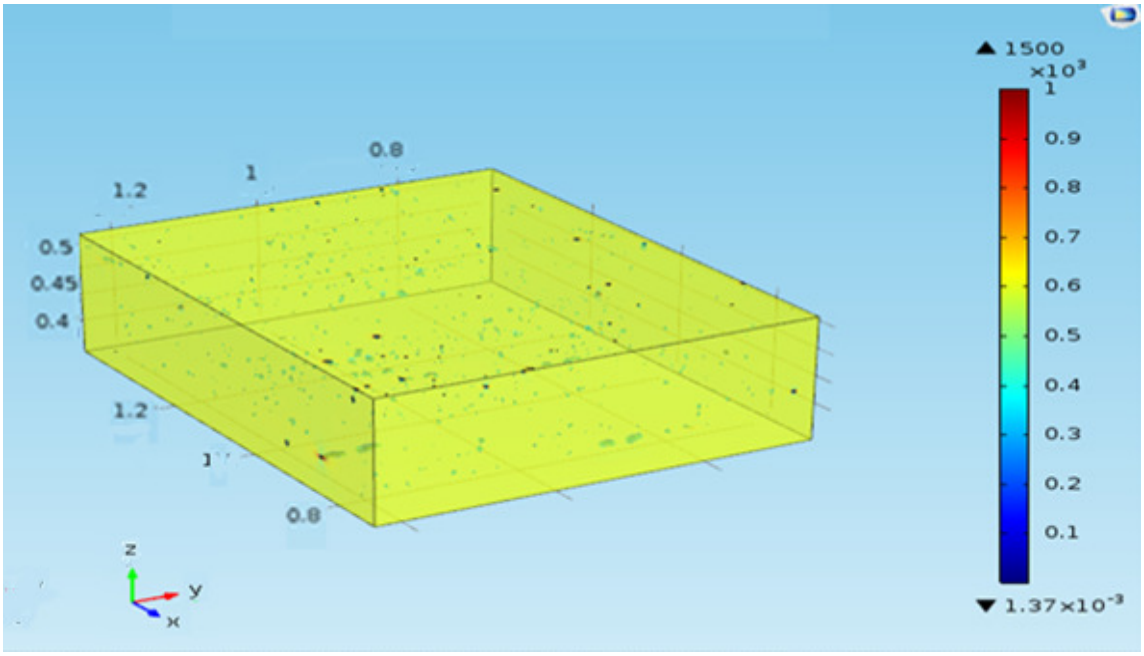


Figure 6.5 Current density (A/m$^2$) on undamaged sample after passing 2A/sq inch current in x direction

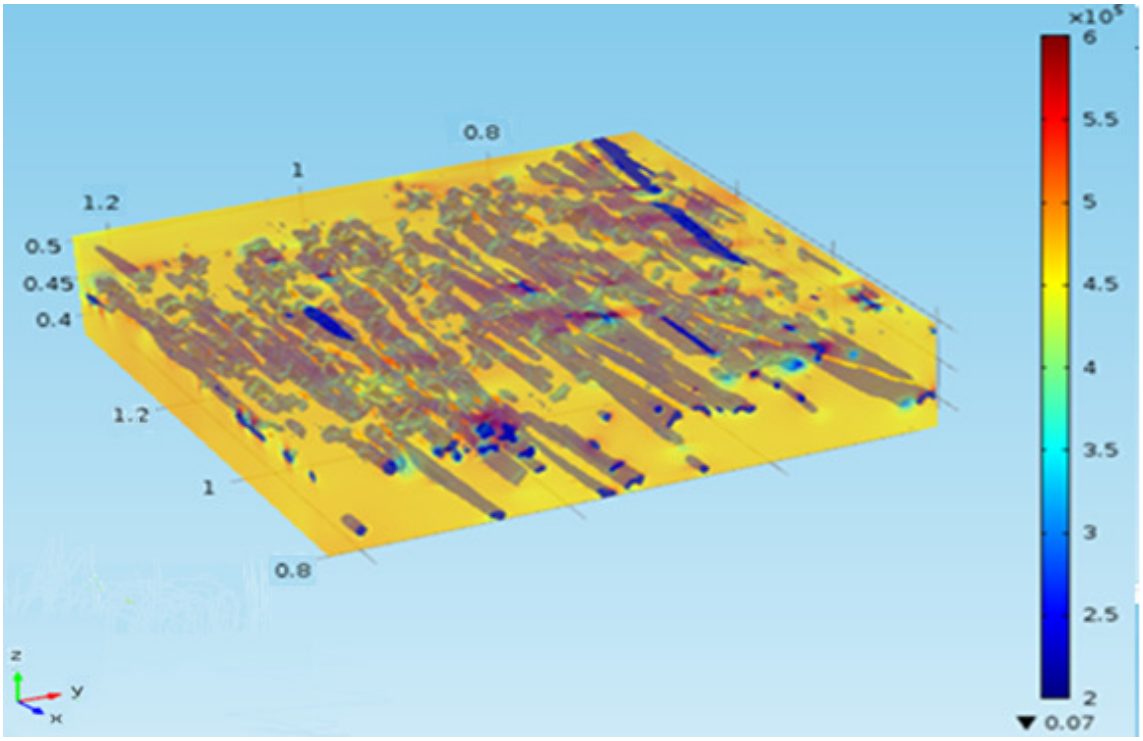


Figure 6.6 Current density (A/m$^2$) on damage sample after passing 30A/sq inch current in x direction

Figure 6.5 shows the surface current density of undamaged sample with manufacturing defects. The current density over the volume is constant except the defect region. Charges are accumulated around the damage and causes high current density.

Figure 6.6 shows the surface current density of a damaged sample. The damage was experimentally created after passing 30A/sq. inch. In the FEA the same amount of current intensity is provided to investigate the effect of evolving material state. At 30A/ sq. inch, there is significant amount of damage. The current density inside the damage area is quite low as the damage area is not good electrical conductor compared to the surrounding area. There is a big mismatch in electrical conductivity at the damaged boundary. The charges are accumulated at the damage boundary and cause high current density.

### 6.2.3 Temperature Distribution

The coupled thermal-electrical FEA model is adopted for the thermography simulation using the same study as in the electrical potential distribution. The temperature distribution is simulated by Joule heating coupling. Thus, damage leads to significant change in temperature distribution. When the temperature distributions are compared to those of the experimental measurements they are in good agreement. Figure 6.7 and Figure 6.8 show the temperature distribution of undamaged sample and damaged sample, respectively. It can be seen the there are some localized areas associated with damage where current density is much higher than in other area. Those localized areas experience higher temperature than the surrounding which ultimately leads to further damage growth or evolution of damage.

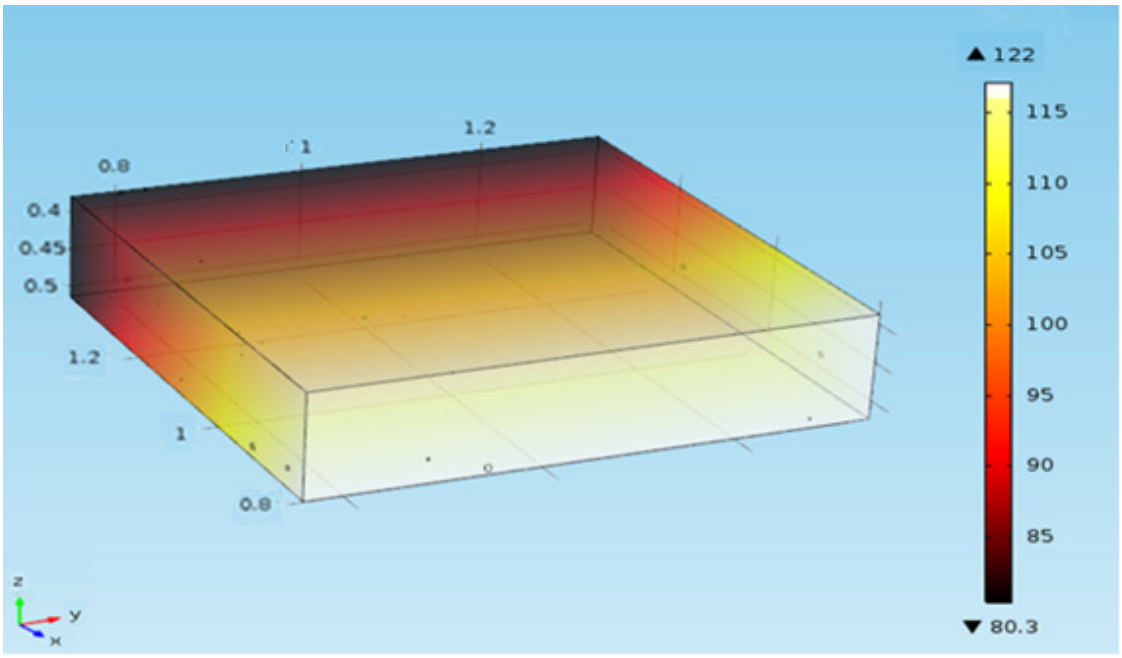


Figure 6.7 Temperature distribution (T) on undamaged sample after passing 30A/sq inch current in x-direction.

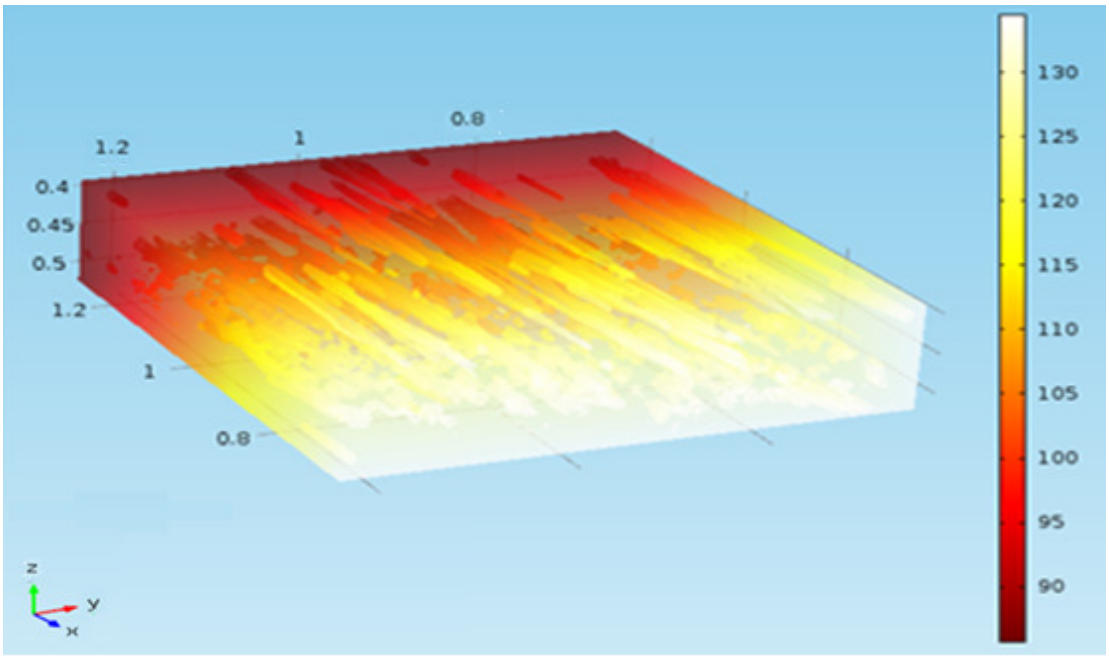


Figure 6.8 Temperature distribution (T) on damaged sample after passing 30A/sq inch current in x-direction.

# CHAPTER 7
# ESTIMATION OF ELECTRICAL CONDUCTIVITY OF A TRANSVERSELY ISOTROPIC LAMINA

As discussed in earlier chapters, electrical behavior of composite materials is clearly not isotropic. The behavior can be orthotropic in material coordinate system (at the lamina scale) and anisotropic in global coordinate system (at the laminate scale) with significant off-diagonal conductivity components. There is strong dependence on fiber orientation angle which not only affects bulk laminate properties but also controls local lamina nonlinear behavior. For a comprehensive understanding of electrical response, the role of the local geometries and properties of the individual constituents needs to be quantified.

Experimental and analytical estimation of electrical properties of composite materials has attracted a significant interest in the recent years. The electrical conductivity of two phase composite media has been studied by various researchers [50]-[52]. Electrical resistivity prediction of dry carbon fiber media as a function of thickness and fiber volume fraction combining empirical and analytical formulation has also been reported [51]. An experimental investigation of through-thickness electrical resistivity of carbon fiber reinforced laminates has been conducted by Louis et al.[53]. Ezquerra et al. [54] has measured alternating-current electrical properties of carbon-fiber polymeric composites. Y lin et al. [55] has improved through thickness electrical conductivity by adding carbon nanotubes addition in the through-thickness of composite laminates for aircraft applications. Despite progress in this area, there is very limited work on a micromechanics based predictive formulation of electrical properties of composite materials. Specifically,

it is very important to understand how electrical conductivity of a composite lamina is affected by volume fraction, distribution, and orientation of its constituents. This can form a foundation for a more robust constitutive law governing electrical behavior of a composite laminate.

In this chapter, an effective electrical conductivity estimation is performed by developing new micromechanics formulations based on a classical micromechanics technique called concentric cylinder method (CCM). Micromechanics schemes such as the Mori-Tanaka method, the self-consistent method are good approximation methods for composites with a low volume fraction of reinforcements in a resin. [56]. CCM is developed based on the assumption that composites are in a state of periodic arrangement; CCM provides a closed form solution. In this study, CCM has been extended to predict electrical properties and continuity boundary conditions are also preserved in terms of electrical variables. In addition of volume fraction and constituent properties, the formulation can account for other complexities such as interphase which can have a significant role in controlling electrical behavior.

## 7.1 GOVERNING EQUATION

To develop governing equation, we assume that the composite lamina is electrically transversely isotropic, i.e., $\sigma_2 = \sigma_3$ . This is consistent with most micromechanics theories for mechanical properties. It is well understood that although lamina is assumed transversely isotropic, the laminate may not be transversely isotropic.

In cylindrical coordinates $(x, r, \theta)$, the following electrical equilibrium equation can be written for orthotropic materials

$$\sigma_r \frac{\partial^2 \phi}{\partial r^2} + \sigma_\theta \left( \frac{1}{r^2} \frac{\partial^2 \phi}{\partial \theta^2} + \frac{1}{r} \frac{\partial \phi}{\partial r} \right) + \sigma_x \left( \frac{\partial^2 \phi}{\partial x^2} \right) = 0 \tag{7-1}$$

Here, $\sigma$ = electrical conductivity and $\phi$ = electric potential function.

To evaluate conductivity in axial (fiber direction) and transverse (perpendicular to fiber direction) direction the following cases are considered.

In axial direction: $\phi = \phi(x)$ and in transverse direction: $\phi = \phi(r, \theta)$

Axis *x* is an arbitrary radial direction along which the electrical conductivity is constant.

We make a major simplifying assumption that the electrical potential function can be written as $\phi(x, r, \theta) = X(x) R(r) \Theta(\theta)$. Hence the governing equation (7-1) can be expressed as

$$\sigma_z \left( \frac{\partial^2 X}{\partial x^2} \right) = 0 \tag{7-2}$$

$$\frac{\partial^2 R}{\partial r^2} \Theta + \left( \frac{1}{r^2} \frac{\partial^2 \Theta}{\partial \theta^2} R + \frac{1}{r} \frac{\partial R}{\partial r} \Theta \right) = 0 \tag{7-3}$$

Solution of equations (7-2) and (7-3) are respectively

$$X(x) = Ax + B \tag{7-4}$$

$$R(r) = \left( Cr + \frac{1}{r} D \right); \Theta(\theta) = cos\theta \tag{7-5}$$

Where *A, B, C, D* are constants to be determined from boundary and/or interface conditions.

## 7.2 TWO PHASE CONCENTRIC CYLINDERS METHOD (CCM)

The composite cylinder assemblage of Figure 7.1.is embedded with two phases whose material properties are the same as the material properties of the effective solid homogeneous material of Figure 7.1. Constant A, B, C, D from equation (7-4) and (7-5) can be found from two-phase composite cylinders model.

### 7.2.1 Axial (fiber direction) Conductivity

The two-phase CCM is used to determine the effective axial conductivity consists of two concentric cylinders or phases (Figure 7.1), each of which is assumed to have material symmetry and has potential of the form.

$$\phi^f = A^f x + B^f \ for 0 \le r \le r_f \tag{7-6}$$

$$\phi^m = A^m x + B^m \ for r_f \le r \le r_m \tag{7-7}$$

Where, superscript *f*= fiber and superscript *m*= matrix

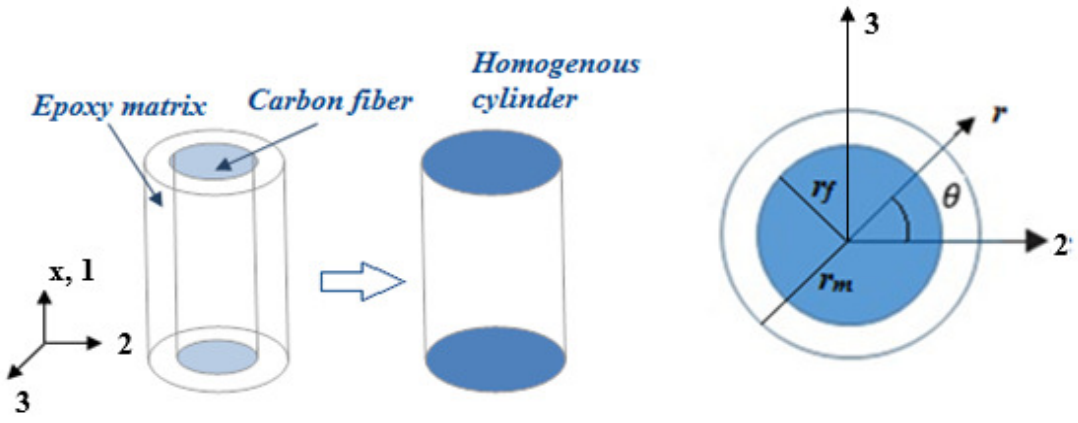


Figure 7.1 Two phase concentric composite cylinders model

Boundary Condition: the following boundary condition is imposed in order to determine the axial conductivity

$$\phi^{f,m}\left(x=-\frac{L}{2}\right)=\phi_0 \tag{7-8}$$

$$\phi^{f,m}\left(x=\frac{L}{2}\right)=\phi_0+\Delta\phi \tag{7-9}$$

By using boundary condition equation (7-8) and (7-9), equation (7-6) and (7-7) gives the following values

$$A^f = A^m = \frac{\Delta\phi}{L} \tag{7-10}$$

$$B^f = B^m = \phi_0 + \frac{\Delta\phi}{2} \tag{7-11}$$

Thus the nonzero electric field component in each phase is determined to be

$$E_x{}^{f,m} = -\frac{\partial\phi^{f,m}}{\partial x} = -A^{f,m} \tag{7-12}$$

The nonzero current flux in axial direction is

$$J_x{}^{f,m} = \sigma^{f,m}E_x{}^{f,m} = -\sigma^{f,m}A^{f,m} \tag{7-13}$$

The axial conductivity $\sigma_1$ can be expressed as following equation

$$\sigma_1 = \frac{J_x}{E_x} \tag{7-14}$$

The current flux $J_z$ is the spatial average of the electric current density along the $x$ axis

$$J_x = \frac{1}{V}\iiint J_x{}^{f,m}dV \tag{7-15}$$

The electric field can be written as

$$E_x = E_x^{\,f} = E_x^{\,m} = -\frac{\Delta\phi}{L} \tag{7-16}$$

Using equation (7-15) and (7-16) into equation (7-14) the following expression can be written

$$\sigma_1 = \frac{\frac{1}{V}\iiint J_x^{\,f,m} dV}{E_x} \tag{7-17}$$

$$\frac{1}{V}\iiint J_x^{\,f,i,m} dV = \frac{1}{V}[\iiint J_x^{\,f} dV + \iiint J_x^{\,i} dV + \iiint J_x^{\,m} dV] \tag{7-18}$$

Here, $V = \pi r_m^{\,2} z$ and $dV = r\,dr d\theta dz$. After solving equation (7-17), the axial conductivity $\sigma_1$.can be found as

$$\sigma_1 = \left[\sigma^f V_f + \sigma^m (1 - V_f)\right] \tag{7-19}$$

Here, $V_f$ = fiber volume fraction. This CCM based axial conductivity equation has the form of the classical rule of mixture model (ROM). The outcome is expected be reasonable as current flow is quite unidirectional and dominated by conduction path provided by the fibers.

### 7.2.2 Transverse Conductivity

Due to the variation of the cylindrical surface area in the transverse direction, the law-of mixture rule is not applicable for calculating the electrical conductivity in this direction. In order to determine the transverse electrical conductivity $\sigma_2$, the system is subjected to uniform electric field $E_0$ along 2 direction at a large distance sufficiently far away (Figure 7.2). The two phase composite cylinder assemblage used to determine the effective

transverse conductivity consists of two concentric cylinders or phases (Figure 7.1), each of which is assumed to have material symmetry and has a potential of the form

$$\phi^f = \left( C^f r + \frac{1}{r} D^f \right) cos\theta \quad for\, 0 \le r \le r_f \tag{7-20}$$

$$\phi^m = \left( C^m r + \frac{1}{r} D^m \right) cos\theta \;\; for\, r_f \le r \le r_m \tag{7-21}$$

Where, superscript *f*= fiber and superscript *m*= epoxy matrix

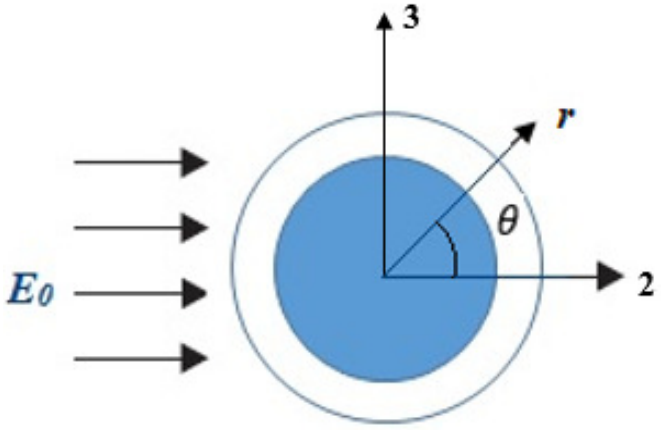


Figure 7.2 Two phase composite cylinder assemblage under electric field

The following boundary condition has been applied in order to determine the axial conductivity: At *r = 0* potential should have finite value; hence, $D^f = 0$.

To enforce continuity of current and potential across the material boundary, the boundary conditions are

$$\phi^f \mid_{r=r_f} = \phi^m \mid_{r=r_f} \tag{7-22}$$

$$J^f \mid_{r=r_f} = J^m \mid_{r=r_f} \tag{7-23}$$

Equation (7-23) can also be written as

$$\sigma_f \frac{\partial \phi^f}{\partial r}|_{r=r_f} = \sigma_m \frac{\partial \phi^m}{\partial r}|_{r=r_f} \tag{7-24}$$

Boundary condition at $r = r_m$

$$-\frac{\partial \phi^m}{\partial r}|_{r=r_m} = E_0 \cos\theta \tag{7-25}$$

or

$$\phi^m|_{r=r_m} = -E_0 r_m \cos\theta \tag{7-26}$$

From equations (7-22), (7-24) and (7-26), the constant $C^f$, $C^m$, $D^m$ can be found as the solution of the following equation

$$\begin{bmatrix} 1 & -1 & -\frac{1}{r_f^2} \\ 1 & -\frac{\sigma_m}{\sigma_f} & \frac{1}{r_f^2}\frac{\sigma_m}{\sigma_f} \\ 0 & 1 & \frac{1}{r_m^2} \end{bmatrix} \begin{bmatrix} C^f \\ C^m \\ D^m \end{bmatrix} = \begin{bmatrix} 0 \\ 0 \\ -E_0 \end{bmatrix} \tag{7-27}$$

After solving the above equation for coefficients $C^f$, $C^m$, $D^m$, the electric potential can be found from equation (7-20) and (7-21)

$$\phi^f = -\frac{2\sigma_m E_0 r \cos\theta}{\sigma_m(1+v_f)+(1-v_f)\sigma_f} \tag{7-28}$$

$$\phi^m = -\left[\frac{\sigma_m + \sigma_f}{\sigma_m(1+v_f)+(1-v_f)\sigma_f} + \frac{1}{r^2}\frac{(\sigma_m - \sigma_f)r_f^2}{\sigma_m(1+v_f)+(1-v_f)\sigma_f}\right] E_0 r \cos\theta \tag{7-29}$$

Electric field and current flux can be found from the following expression

$$E_r^{f,m} = -\frac{\partial \phi^{f,m}}{\partial r} \tag{7-30}$$

$$J_r^{f,m} = \sigma E_r^{f,m} \tag{7-31}$$

$$E_\theta^{f,m} = -\frac{\partial \phi^{f,m}}{\partial \theta} \tag{7-32}$$

$$J_\theta^{f,m} = \sigma E_\theta^{f,m} \tag{7-33}$$

Transverse conductivity can be express as

$$\sigma_2 = \frac{J_2}{E_0} = \frac{\frac{1}{V}\iiint J_2^{f,m} dV}{E_0} \tag{7-34}$$

Where,

$$\frac{1}{V}\iiint J_2^{f,m} dV = \frac{1}{V}[\iiint (J_r^f \cos\theta - J_\theta^f \sin\theta) dV + \iiint (J_r^m \cos\theta - J_\theta^m \sin\theta) dv] \tag{7-35}$$

From equation (7-34) and (7-35), one gets

$$\sigma_2 = \sigma^m \frac{\left[\sigma^f (1+V_f) + \sigma^m (1-V_f)\right]}{\left[\sigma^f (1-V_f) + \sigma^m (1+V_f)\right]} \tag{7-36}$$

Equation (7-36) is the micromechanical relationship for predicting electrical conductivity of a lamina in the transverse (perpendicular to fiber) directions.

### 7.3 THREE PHASE CONCENTRIC CYLINDERS METHOD (CCM)

Three phase composite cylinder assemblage as shown in Figure 7.3 is embedded by three phases whose material properties are the same as the material properties of the effective

solid homogeneous material. Constant A, B, C, D from equation (7-4) and (7-5) can be found from the three phase composite cylinders model.

### 7.3.1 Axial Conductivity

The three-phase composite cylinder assemblage used to determine the effective axial conductivity consists of three concentric cylinders or phases (Figure 7.3) each of which is assumed to have isotropic material symmetry and has a potential of the form

$$\phi^f = A^f x + B^f \ for 0 \le r \le r_f \tag{7-37}$$

$$\phi^i = A^i x + B^i \ for r_f \le r \le r_i \tag{7-38}$$

$$\phi^m = A^m x + B^m \ for r_i \le r \le r_m \tag{7-39}$$

Where, *f*= fiber, *m*= epoxy matrix and *i*=interphase

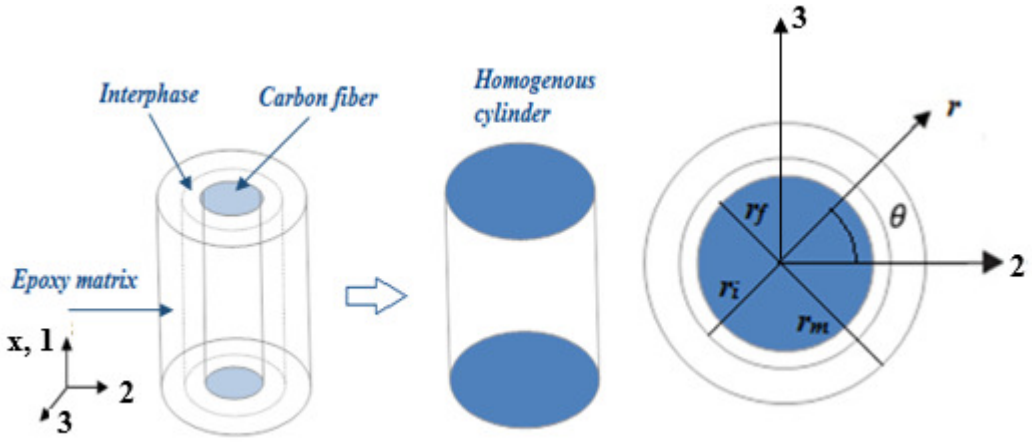


Figure 7.3 Three phase concentric composite cylinders model

Boundary Condition: the following boundary condition is imposed in order to determine the axial conductivity

$$\phi^{f,i,m}\left(x=-\frac{L}{2}\right)=\phi_0 \tag{7-40}$$

$$\phi^{f,i,m}\left(x=\frac{L}{2}\right)=\phi_0+\Delta\phi \tag{7-41}$$

By using the boundary condition (7-40), (7-41) and equation (7-37), (7-38) and (7-39) the following constants can be found

$$A^f = A^i = A^m = \frac{\Delta\phi}{L} \tag{7-42}$$

$$B^f = B^i = B^m = \phi_0 + \frac{\Delta\phi}{2} \tag{7-43}$$

Thus, the nonzero electric field component in each phase is determined to be

$$E_x{}^{f,i,m} = -\frac{\partial\phi^{f,m}}{\partial x} = -A^{f,i,m} \tag{7-44}$$

The nonzero current flux is

$$J_x{}^{f,i,m} = \sigma^{f,i,m}E_x{}^{f,m} = -\sigma^{f,i,m}A^{f,i,m} \tag{7-45}$$

The axial conductivity can be expressed as following equation

$$\sigma_1 = \frac{J_x}{E_x} \tag{7-46}$$

The current flux $J_z$ is the spatial averages of the electric current density along the $z$ axis

$$J_x = \frac{1}{V}\iiint J_x{}^{f,i,m}\,dV \tag{7-47}$$

And electric field can be written as follow

$$E_x = E_x^{\,f} = E_x^{\,i} = E_x^{\,m} = -\frac{\Delta\phi}{L} \tag{7-48}$$

Using equation (7-47) and (7-48) into equation (7-46) the following expression can be written

$$\sigma_1 = \frac{J_x}{E_x} = \frac{\frac{1}{V}\iiint J_x^{\,f,i,m} dV}{E_x} \tag{7-49}$$

$$\frac{1}{V}\iiint J_x^{\,f,i,m} dV = \frac{1}{V}\left[\iiint J_x^{\,f} dV + \iiint J_x^{\,i} dV + \iiint J_x^{\,m} dV\right] \tag{7-50}$$

Here, $V = \pi r_m^{\,2} z \;\; and \;\; dV = r\, dr d\theta dz$

$$\sigma_1 = \left[\sigma^f V_f + \sigma^i V_i + \sigma^m (1 - V_f - V_i)\right] \tag{7-51}$$

Here $V_i$ = interphase volume fraction. This is rule of mixture of axial conductivity.

### 7.3.2 Transverse Conductivity

Due to the variation of the cylindrical surface area in the transverse direction, the law-of mixture rule is not applicable for calculating the electrical conductivity in this direction. In order to determine the transverse electrical conductivity $\sigma_2$, the system is subjected to uniform electric field $E_0$ along 2 direction at a large distance sufficiently far away (Figure 7.4) . The three phase composite cylinder assemblage is used to determine the effective transverse conductivity consists of three concentric cylinders or phases (Figure 7.3), each of which is assumed to have isotropic material symmetry and has a potential of the form

$$\phi^f = \left(C^f r + \frac{1}{r} D^f\right) cos\theta \quad for\, 0 \le r \le r_f \tag{7-52}$$

$$\phi^i = \left( C^i r + \frac{1}{r} D^i \right) cos\theta \quad for\, r_f \le r \le r_i \tag{7-53}$$

$$\phi^m = \left( C^m r + \frac{1}{r} D^m \right) cos\theta \quad for\, r_i \le r \le r_m \tag{7-54}$$

Where, *f*= fiber, *i*= interphase *and m*= epoxy matrix

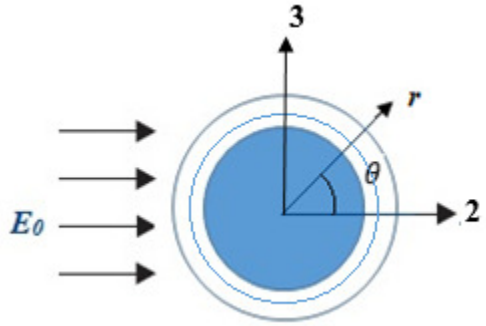


Figure 7.4 Three phase composite cylinder assemblage under electric field

The following boundary condition is imposed in order to determine the axial conductivity:

At $r = 0$ potential should have finite value; hence, $D^f = 0$

From continuity equation,

$$\phi^f \mid_{r=r_f} = \phi^i \mid_{r=r_f} \tag{7-55}$$

$$J^f \mid_{r=r_f} = J^i \mid_{r=r_f} \tag{7-56}$$

or,
$$\sigma_f \frac{\partial \phi^f}{\partial r} \mid_{r=r_f} = \sigma_i \frac{\partial \phi^i}{\partial r} \mid_{r=r_f} \tag{7-57}$$

$$\phi^i \mid_{r=r_i} = \phi^m \mid_{r=r_i} \tag{7-58}$$

$$J^i|_{r=r_i} = J^m|_{r=r_i} \tag{7-59}$$

or

$$\sigma_i \frac{\partial \phi^i}{\partial r}|_{r=r_i} = \sigma_m \frac{\partial \phi^m}{\partial r}|_{r=r_i} \tag{7-60}$$

Boundary condition at $r=r_m$,

$$-\frac{\partial \phi^m}{\partial r}|_{r=r_m} = E_0 \cos\theta \tag{7-61}$$

or

$$\phi^m|_{r=r_m} = -E_0 r_m \cos\theta \tag{7-62}$$

By using continuity equations, boundary conditions, and equation (7-52), (7-53) and (7-54) the following equations can be written

$$\begin{bmatrix} 1 & -1 & -\frac{1}{r_f^2} & 0 & 0 \\ -1 & -\frac{\sigma_i}{\sigma_f} & -\frac{1}{r_f^2}\frac{\sigma_i}{\sigma_f} & 0 & 0 \\ 0 & 1 & \frac{1}{r_i^2} & -1 & -\frac{1}{r_i^2} \\ 0 & -1 & \frac{1}{r_i^2} & \frac{\sigma_m}{\sigma_i} & -\frac{1}{r_i^2}\frac{\sigma_m}{\sigma_i} \\ 0 & 0 & 0 & 1 & \frac{1}{r_m^2} \end{bmatrix} \begin{bmatrix} c^f \\ c^i \\ d^i \\ c^m \\ d^m \end{bmatrix} = \begin{bmatrix} 0 \\ 0 \\ 0 \\ 0 \\ -E_0 \end{bmatrix} \tag{7-63}$$

After solving the above equation and using equations (7-52), (7-53) and (7-54), the electric field and current flux can be found as

$$E_r^{f,i,m} = -\frac{\partial \phi^{f,i,m}}{\partial r} \tag{7-64}$$

$$J_r^{f,i,m} = \sigma E_r^{f,i,m} \tag{7-65}$$

$$E_\theta^{f,i,m} = -\frac{\partial \phi^{f,i,m}}{\partial \theta} \tag{7-66}$$

$$J_\theta^{f,i,m} = \sigma E_\theta^{f,i,m} \tag{7-67}$$

Transverse conductivity can be calculated from following equation

$$\sigma_2 = \frac{J_2}{E_0} = \frac{\frac{1}{V}\iiint J_2^{f,i,m} dV}{E_0} \tag{7-68}$$

where

$$\frac{1}{V}\iiint J_2^{f,m} dV = \frac{1}{V}[\iiint (J_r^f \cos\theta - J_\theta^f \sin\theta) dV + \iiint (J_r^i \cos\theta - J_\theta^i \sin\theta)^{dV} + \iiint (J_r^m \cos\theta - J_\theta^m \sin\theta)^{dV}] \tag{7-69}$$

## 7.4 RESULTS AND DISCUSSION

It should be mentioned that the CCM micromechanics model in the current work is modified based on the assumption of straight carbon fibers which are uniformly distributed in the polymer matrix. The interaction between one fibers to another fiber is neglected this corresponds to the dilute mixture assumption as applied in different effective medium theories. Micromechanics modeling results for the effective axial electrical conductivity and transverse conductivity of two-phase CCM are presented in Figure 7.5-7.6. In these figures, different ratios of fiber to matrix conductivities have been used which indicates the degree of heterogeneity in electrical properties. Figure 7.5 shows the variation of axial electrical conductivity with fiber volume fraction. Equation (7-19) for the axial electrical conductivity is linear in nature that means the axial conductivity directly depends on the amount of carbon fiber and the conductivity of carbon fiber. As the volume fraction of carbon fiber increases the conductivity increases. Matrix is less conductive than carbon

fiber so the values of effective axial conductivity of composite are between the value of matrix conductivity and carbon fiber conductivity.

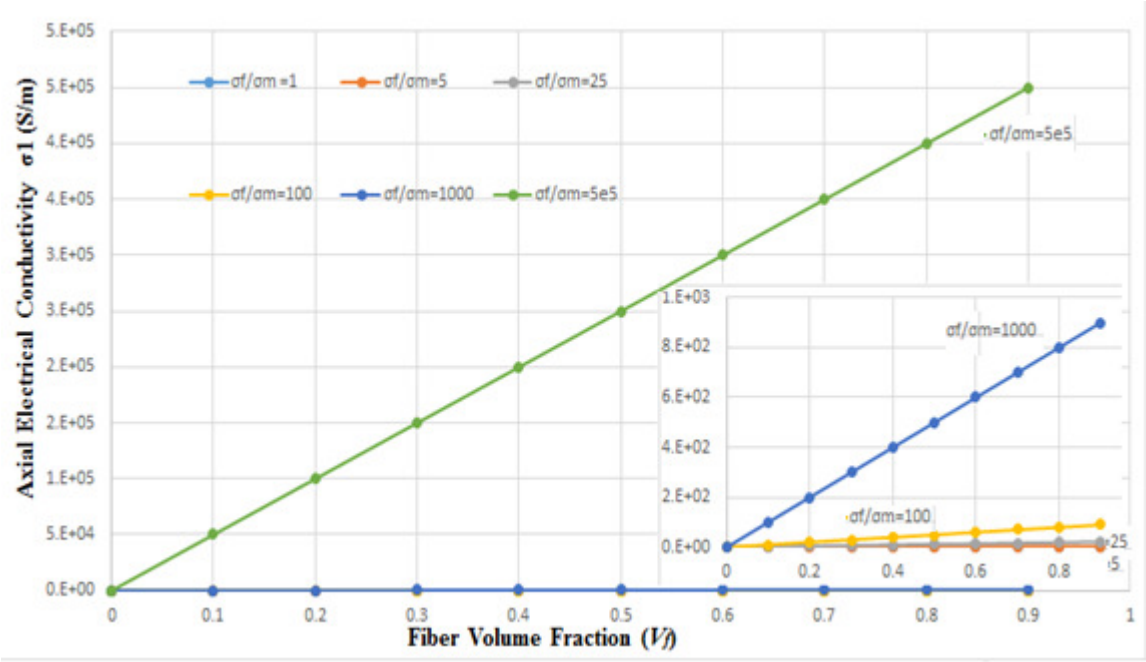


Figure 7.5 Axial Conductivity of two phase composite cylinder model

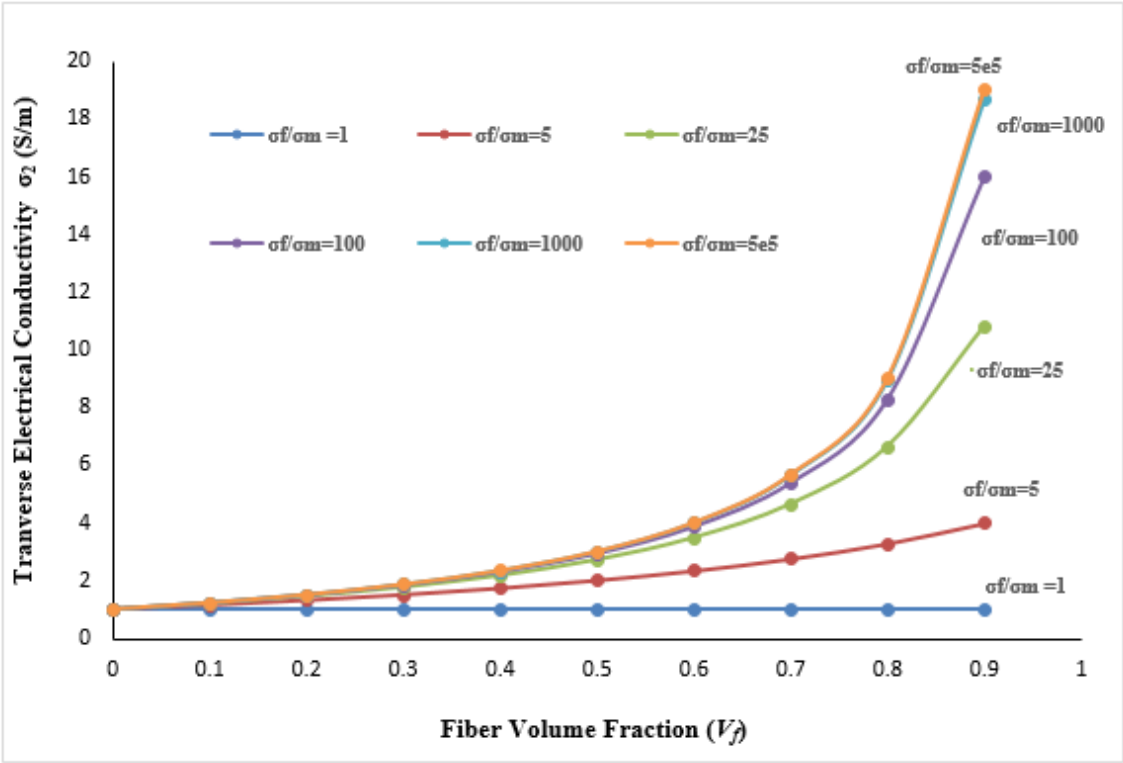


Figure 7.6 Transverse Conductivity of two phase composite cylinder model

Figure 7.6 shows the variation of transverse conductivity of composite materials with fiber volume fraction. In the transverse direction, there is no direct conduction path; hence conductivity is much lower than in the axial direction. There is no significant change in conductivity in transverse direction up to certain 50% fiber volume fraction. As the fiber volume fraction increases the conductivity increases. Figure 7.6 shows different conductivity data for different carbon fiber conductivity to matrix conductivity ratios. At low carbon fiber to matrix conductivity ratio, there is no significant change in effective transverse conductivity of composite with fiber volume fraction. However, as the conductivity ratio increases, the transverse conductivity also increases. It should also be noted that though the transverse conductivity increases with the ratio of fiber conductivity to matrix conductivity, this increase is not significant compared to axial conductivity.

Another fact is that the transverse conductivity increases with the ratio of fiber conductivity to matrix conductivity up to a certain limit. Beyond that limit, there is no significant change in transverse conductivity with carbon fiber to matrix conductivity ratio. It should be mentioned that, for polymeric composites, the fiber-to-matrix conductivity ratio is very high. (For example, for a carbon fiber/epoxy polymer matrix composite, $\sigma f / \sigma m = 1e5$). The transverse electrical conductivity of the composite in such cases changes appreciably only for large fiber volume fractions. Figure 3(b) shows that, for high $\sigma f / \sigma m$ ratios, the contribution of the fiber conductivity only increases substantially for a fiber volume fraction greater than 80%. These fiber volume fractions are not practical and, in many cases, are physically impossible due to the geometry of fiber packing.

Figure 7.7, Figure 7.8, Figure 7.9 and Figure 7.10 Show that variation of axial conductivity of three phase model with different fiber and interphase volume fraction. In the axial direction, the rule of mixture formulation is used. This rule is linear in nature and the total conductivity depends on individual volume fraction and conductivity values. In the axial direction, carbon fiber conductivity is dominant over the others so axial conductivity is increased with increasing carbon fiber volume fraction and fiber to matrix conductivity. By comparing Figure 7.7, Figure 7.8, and Figure 7.9 it can be seen that there is very less significant effect on interphase conductivity and interphase volume fraction on total conductivity.

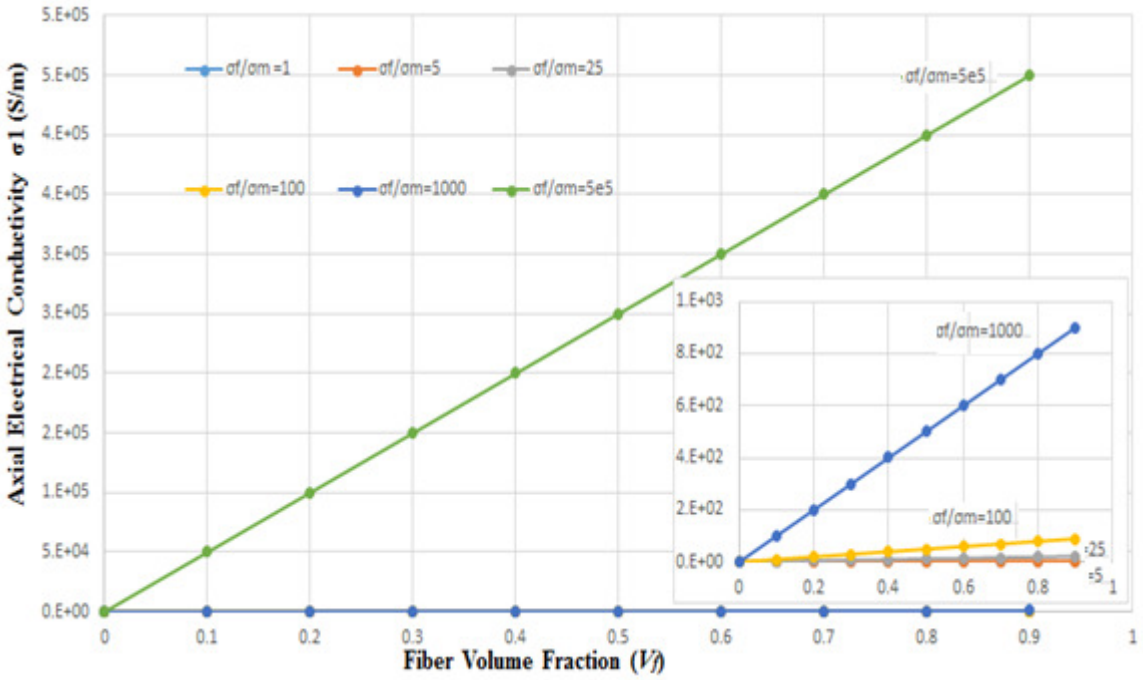


Figure 7.7 Axial Conductivity for three phase model with $\frac{\sigma_i}{\sigma_m}=1$ and $V_i=1\%$

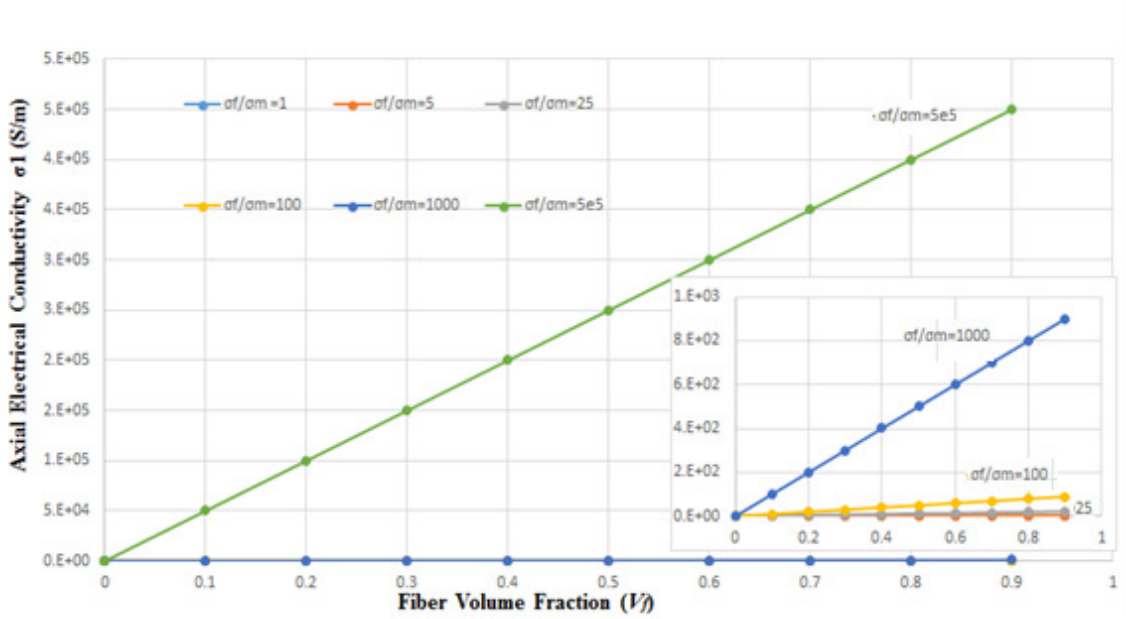


Figure 7.8 Axial conductivity for three phase model with $\frac{\sigma_i}{\sigma_m}=1$ and $V_i=5\%$

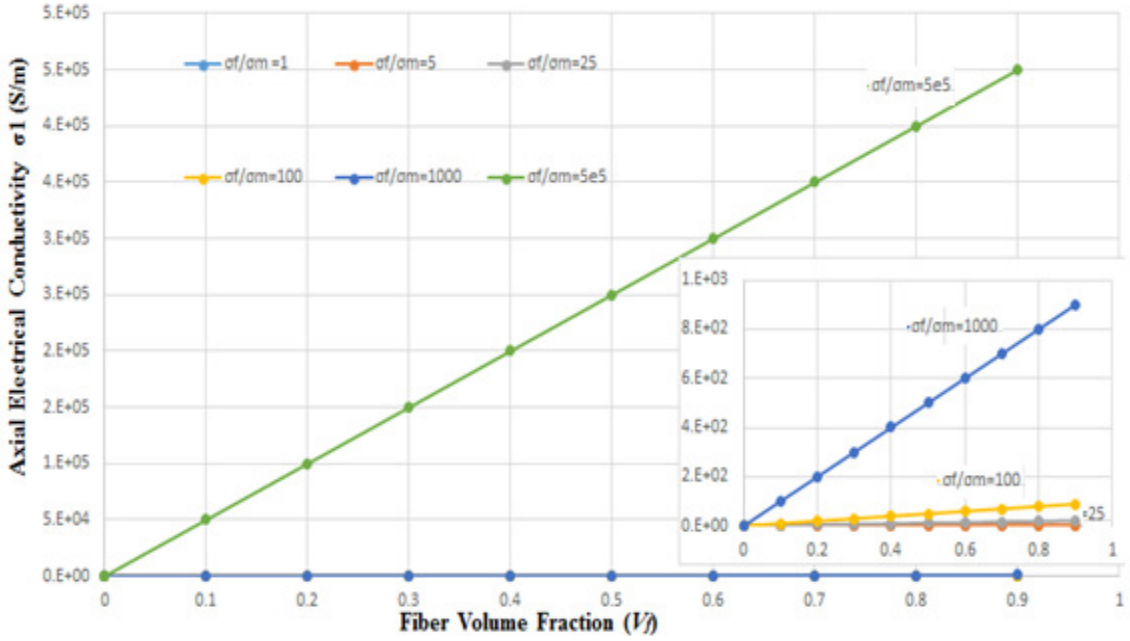


Figure 7.9 Axial conductivity for three phase model with $\frac{\sigma_i}{\sigma_m}=10$ and $V_i=1\%$

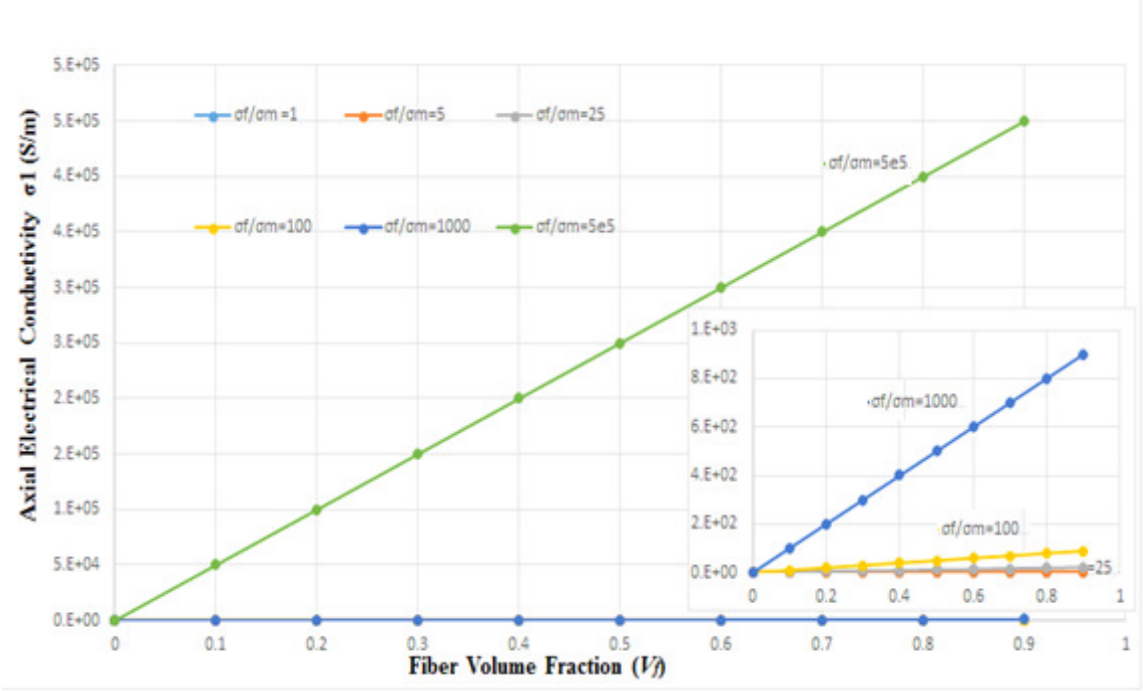


Figure 7.10 Axial conductivity for three phase model with $\frac{\sigma_i}{\sigma_m}=10$ and $V_i=5\%$

Figure 7.11, Figure 7.12, Figure 7.13, and Figure 7.14 show the variation of transverse conductivity of three phase model with different fiber and interphase volume fraction. In transverse direction, there is no direct conduction path; hence the total conductivity values depend on all individual component. Volume fraction and conductivity of individual constituents has significant effect on transverse conductivity. Figure 7.11 shows the effect of fiber volume fraction and fiber conductivity on the transverse conductivity. Transverse conductivity increases with fiber conductivity and fiber volume fraction when fiber to matrix conductivity ratio is more than 1. By comparing Figure 7.11 and Figure 7.13 it can be seen that if the interphase to matrix conductivity ratio is low, then there is no significant change in transverse conductivity with interphase volume fraction. And by comparing Figure 7.11, Figure 7.12 and Figure 7.13, it can be said that transverse conductivity increases with increasing interphase conductivity and, if the volume fraction of interphase is increased, then the transverse conductivity value is also increased (Figure 7.14). The matrix and interphase conductivity can be increased easily by mixing conductive nanomaterials (carbon nanotube, carbon nanofiber, nickel or silver nanoparticle) with the matrix. Modification of interphase is important to enhance transverse conductivity and it may have a more significant role in nonlinear behavior. It should be noted that increasing volume fraction of interphase is not recommended because the mechanical strength may be compromised. Interphase region needs to be within certain limit for proper load transfer from fiber to matrix and to keep interfacial strength high.

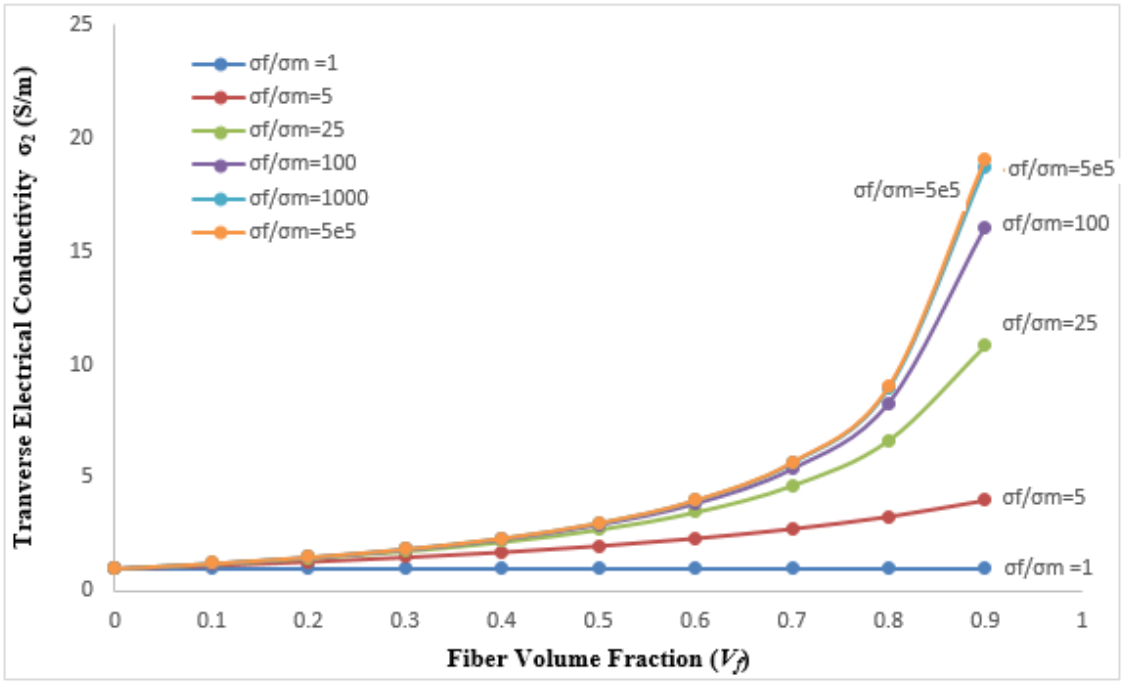


Figure 7.11 Transverse conductivity for three phase composite model with $\frac{\sigma_i}{\sigma_m}=1$ and $V_i=1\%$

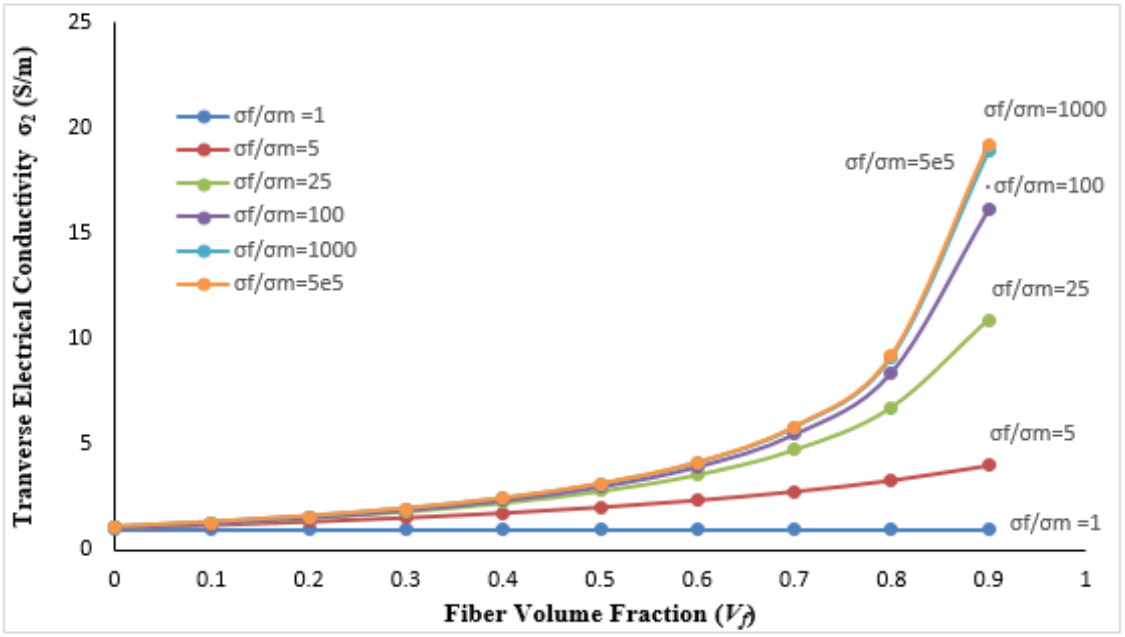

Figure 7.12 Transverse conductivity for three phase composite model with $\frac{\sigma_i}{\sigma_m}=1$ and $V_i=5\%$

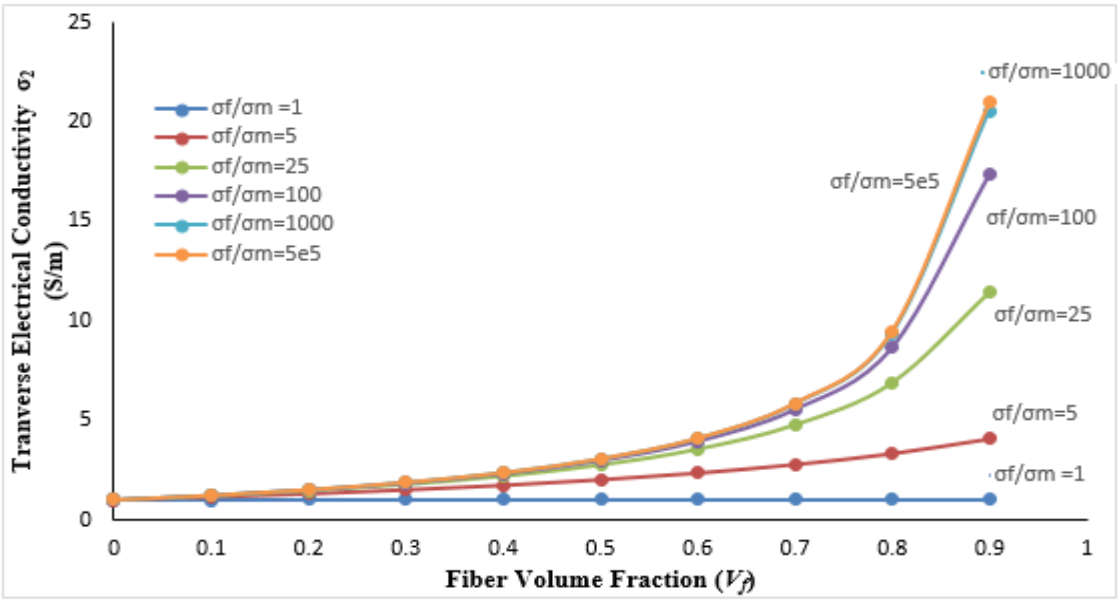


Figure 7.13 Transverse conductivity for three phase composite model with $\frac{\sigma_i}{\sigma_m}=10$ and $V_i=1\%$

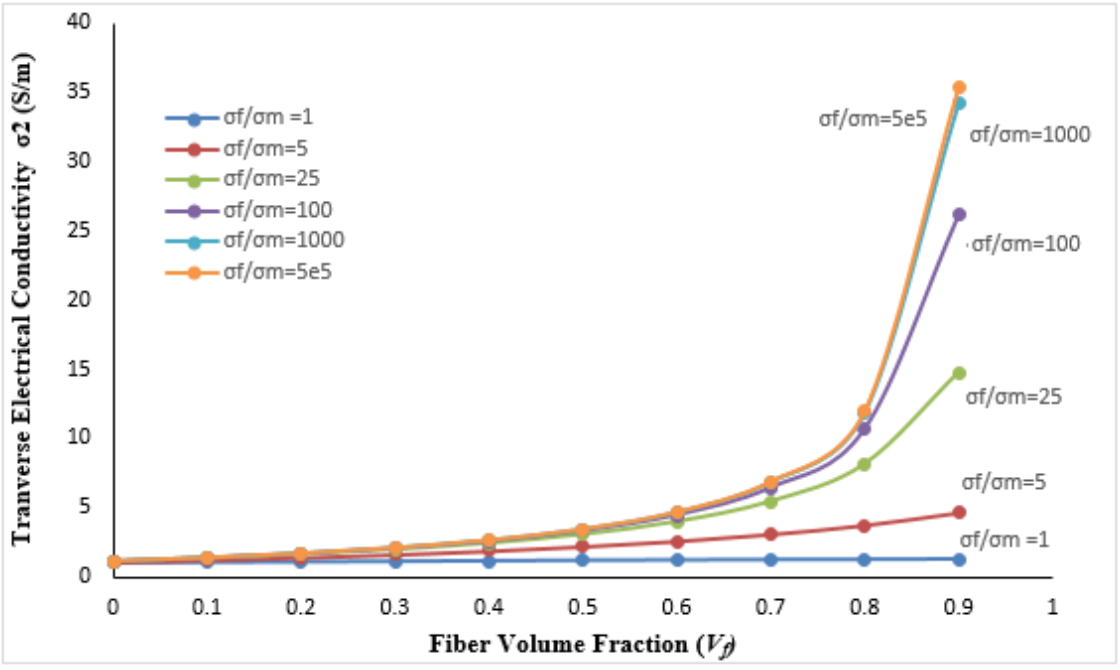

Figure 7.14 Transverse conductivity for three phase composite model with $\frac{\sigma_i}{\sigma_m} = 10$ and $V_i = 5\%$

# CHAPTER 8
# CONCLUSION

In this research work, we utilized broadband dielectric spectroscopy (BbDS) of different heterogeneous material systems to understand the relationship between the internal microstructural mechanisms in the material and the electrical properties. Experimental results show that electrical properties are indeed dependent on laminate design and fiber orientation in the laminate. Electrical effects are often coupled with the structural integrity and the thermal behavior due to "Joule heating" in the composite parts and in their joints. Thermal-electrical properties also depend on progressive increase in current intensity. Electrical current can cause significant damage in the dielectric matrix material while conducting through the fibers. Thus ultimately causes significant change in the electrical properties due to material state changes. 3D image of X-ray microscopy is used to visualize (down to 1 micron) such local material state changes. A finite element analysis on real micro-structure is carried out to understand the electrical-thermal coupling response on evolving material state.

Damage due to electrical load is much more complex than due to pure mechanical load because of the multi-physics coupling behavior. Electrical load is responsible for changing the material state which ultimately affects the electrical response and mechanical response. Materials under service may not perform as expected due to electric current loads. It has also been studied that synergistic mechanical and electrical loading cause material to respond faster than individual loading. Prior mechanical damage influence the

degradation due to electrical response; therefore a previously damaged composite loses its strength faster. It is important to understand how multi-physics properties (e.g. strength, impedance) depend on local details (e.g. micro-structure). This thesis has explored how electrical current is related to material architecture and damage development. Electrical/ mechanical properties measurements were carried out with different current intensity.

Summary of major observations are:

1) Electrical properties depend heavily on the available conduction path (fiber orientation) in the laminate and also laminate design.
2) Increasing current intensity beyond a threshold value can induce irreversible damage in the laminate and such threshold value depends on the laminate architecture.
3) Electrical effects are coupled with thermal behavior due to “Joule heating” and cause significant damage in composite ply.
4) Electrical load is responsible only for changing the material state which ultimately affects the electrical response and mechanical response.
5) Materials respond and degrade differently under synergistic electrical and mechanical loads
6) 3D X-ray imaging validated the fact that Broadband dielectric spectroscopy can be used to calculate impedance and this represents the current state of the material.
7) The material state depends heavily on coupled thermal-electrical effect and when the temperature distributions are compared to those of the electrical measurements and finite element analysis, they are in good agreement in locating the damage.

A micromechanics model is developed to assess the impact of the fiber volume fraction and the electrical conductivity of fiber and matrix on the electrical conductivity of polymer composites. The micromechanics model is used to qualitatively identify the potential causes for how volume fraction changes in conductivity both in the axial direction and in the transverse direction. From the micromechanics model, it is observed that the axial conductivity of carbon fiber composite directly depend on fiber volume fraction and electrical conductivity. The transverse electrical conductivity of composite materials would changed significantly for fiber volume fraction greater than 80%, but this would be unrealistic. Transverse conductivity is matrix dominated and may have greater role in nonlinear behavior. Due to high fiber-to-matrix conductivity ratio, there is no significant improvement of conductivity in transverse direction compared to axial conductivity.

## REFERENCES


[1] Talreja, R. (2008) "Damage and fatigue in composites-A personal account." *Composites Science and Technology*, 2008. 68(13): p. 2585-2591.

[2] Reifsnider, K.L., and Case, S. W. (2002) "Damage Tolerance and Durability of Material Systems." 2002, New Tork: John Wiley & Sons, Inc.

[3] Reifsnider, K.L. (1986) "The critical element model: A modeling philosophy." *Engineering Fracture Mechanics*, 1986. 25(5-6): p. 739-749.

[4] Subramanian, S., Reifsnider, K.L., and Stinchcomb, W.W. (1995) "A cumulative damage model to predict the fatigue life of composite laminates including the effect of a fibre-matrix interphase." *International Journal of Fatigue*, 1995. 17(5): p. 343-351.

[5] Reifsnider, K.L., et al. (2009) "Material state changes as a basis for prognosis in aeronautical structures." *Aeronautical Journal*, 2009. 113(1150): p. 789-798.

[6] Tamuzs, V., Dzelzitis, K., and Reifsnider, K. (2008) "Prediction of the cyclic durability of woven composite laminates." *Composites Science and Technology*, 2008. 68(13): p. 2717-21.

[7] Xing, L., Reifsnider, K.L., and Huang, X. (2009) "Progressive damage modeling for large deformation loading of composite structures." *Composites Science and Technology*, 2009. 69(6): p. 780-4.

[8] Fish, J., et al. (2012) “Multiscale fatigue life prediction model for heterogeneous materials”. *International Journal for Numerical Methods in Engineering*, 2012. 91: p. 1087-1104.

[9] Fazzino, P.D., Reifsnider, K.L., and Majumdar, P. (2009) “Impedance spectroscopy for progressive damage analysis in woven composites.” *Composites Science and Technology*, 2009. 69(11-12): p. 2008-14.

[10] Piascik, B., Vickers, J., Lowry, D., Scotti, S., Stewart, J., and Calomino, A. (2012) Space Technology Roadmaps (TA12): Materials, Structures, Mechanical Systems and Manufacturing in Space Technology Roadmaps. April 2012, NASA.

[11] Tuncer, E., Serdyuk, Y.V., and Gubanski, S.M. (2002) “Dielectric Mixtures: Electrical Properties and Modeling” *IEEE Transactions on Dielectrics and Electrical Insulation*, 2002. 9(5): p. 809-828.

[12] Gibson, R.F. (2010) “A review of recent research on mechanics of multifunctional composite materials and structures.” *Composite Structures*, 2010. 92: p. 2793–2810.

[13] Moupfouma, F. (2011) "Electromagnetic Energy Coupling Mechanism on Cables and Systems - A Comparison Composite Aircraft Versus Metal Aircraft and Impact on Testing Procedure," *SAE Int. J. Aerosp*. 4(2):672-680, 2011, doi:10.4271/2011-01-2513.

[14] Majumdar, P.K.; Haider, M. F.; Reifsnider, K. L. (2013) “AC Conductivity and Microstructural Changes of Composite Materials.” *International Conference on*

*Lightning and Static Electricity (ICOLSE) 2013*, Seattle, Washington, USA. (Hosted by Boeing).

[15] Haider, M. F.; Majumdar, P.K.; Reifsnider, K. L. (2013) "Study of damage in Carbon fiber reinforced Composites Due to Electric Current", *American Society for Composites 28th Technical Conference* September 9-11, 2013 State College, Pennsylvania, USA.

[16] Majumdar, P.K.; Haider, M. F.; Reifsnider, K. L. (2013) "Effect of Fiber Orientation on AC Conductivity of Composite Materials", *SAMPE* 2013 conference, 6-9May, 2013, California, USA.

[17] Majumdar, P.K.; Reifsnider, K.L.; Raihan, Md., R.; Haider, M. F.; "Study of Damage Evolution in Composite Materials Using 3D X-ray Microscope", *SAMPE* 2013 conference, 6-9 May , 2013, California, USA.

[18] Majumdar, P.K.; Haider, M. F; Reifsnider, K. L. (2013) "Multi-Physics Response of Structural Composites and Framework for Modeling using Material Geometry", *54th AIAA/ASME/ASCE/ASC structures, structural Dynamics, and Materials conference*, 8-11 Aprl 2013, Boston, Massachusetts, USA.

[19] Haider, M. F.; Majumdar, P.K.; Angeloni, S.; Reifsnider, K. L. (2015) "Measurement and Prediction of Electrical Response of Composite Materials." *SAMPE 2015 conference* May 18-21, 2015 Baltimore, Maryland, USA.

[20] Haider, M. F.; Majumdar, P.K.; Angeloni, S., (2015) "Degradation of Carbon Fiber Composite Materials Due to Electrical Current and Potential Impact on Synergistic Durability." *American Society for Composites 30th Technical*

*Conference September* 28-30, 2015 Michigan State University, East Lansing, Michigan, USA.

[21] Ogasawara, T., Hirano, Y., and Yoshimura, A. (2010) "Coupled thermal–electrical analysis for carbon fiber/epoxy composites exposed to simulated lightning current". *Composites: Part A* 2010. 41: p. 973–981.

[22] Feraboli, P. and Miller, M. (2010) "Damage resistance and tolerance of carbon/epoxy composite coupons subjected to simulated lightning strike." *Composites: Part A* 2009. 40: p. 954–967.

[23] Gou, J., Tang, Y., Liang, F., Zhao, Z., Firsich, D., and Fielding, J. (2010). Carbon nanofiber paper for lightning strike protection of composite materials. Composites Part B: Engineering, 41(2), 192-198.

[24] Mall, S. and Ouper, B.L. (2009) "Compression Strength Degradation of Nanocomposites after Lightning Strike." *Journal of Composite Materials*, 2009. 43(24).

[25] Makvandi, R, and Andreas Ö. (2014) "On a Finite Element Approach to Predict the Thermal Conductivity of Carbon Fiber Reinforced Composite Materials." Defect and Diffusion Forum. Vol. 354. 2014.

[26] Miller, A. (2007) The Boeing 787 Dreamliner. Keynote address. In: 22*nd American society for composites technical conference*, Seattle, WA; September 2007.

[27] Kaw, A K. (2005) *Mechanics of composite materials*. CRC press, 2005.

[28] Wen, J.; Xia, Z..; Choy, F., "Damage detection of carbon fiber reinforced polymer composites via electrical resistance measurement", *Composites Part B*: Engineering, Volume 42, Issue 1, January 2011, Pages 77-86.

[29] Reifsnider, K. L.; Ed., "Damage in Composite Materials." ASTM STP 775, American Society for Testing and Materials, Philadelphia 1982.

[30] Reifsnider, K.L., and Case, S. W. (2002), "*Damage Tolerance and Durability of Material Systems*". New York: John Wiley and Sons.

[31] Highsmith, A. L., and Reifsnider, K. L. (1982). "Stiffness-reduction mechanisms in composite laminates." Damage in composite materials, ASTM STP, 775, 103-117.

[32] Nairn, J. A. (2000). "Matrix microcracking in composites." *Polymer Matrix Composites*, 2, 403-432.

[33] Talreja, R. (1985). "Transverse cracking and stiffness reduction in composite laminates." *Journal of Composite Materials*, 19(4), 355-375.

[34] Talreja, R., and Singh, C. V. (2012). "*Damage and failure of composite materials*." Cambridge University Press.

[35] Varna, J., and Krasnikovs, A. (1998). "Transverse cracks in cross-ply laminates 2. Stiffness degradation." *Mechanics of Composite Materials*, 34(2), 153-170.

[36] O'brien, T. K. (1982). "Characterization of delamination onset and growth in a composite laminate." Damage in composite materials, ASTM STP, 775(2), 140-167.

[37] Subramanian, S., Reifsnider, K. L., and Stinchcomb, W. W. (1995). "Tensile strength of unidirectional composites: the role of efficiency and strength of fiber-

matrix interface." *Journal of Composites Rechnology & Research*, 17(4), 289-300.

[38] Razvan, A., and Reifsnider, K. L. (1991). "Fiber fracture and strength degradation in unidirectional graphite/epoxy composite materials." *Theoretical and Applied Fracture Mechanics*, 16(1), 81-89.

[39] Gao, F., Boniface, L., Ogin, S. L., Smith, P. A., & Greaves, R. P. (1999). "Damage accumulation in woven-fabric COMPOSITES laminates under tensile loading: Part 1. Observations of damage accumulation." *Composites Science and Technology*, 59(1), 123-136.

[40] Raihan, M.(2014). "Dielectric Properties of Composite Materials during Damage Accumulation and Fracture." (Doctoral dissertation). Retrieved from http://scholarcommons.sc.edu/etd/2896.

[41] Clifford, J. (2015) "Dielectric characteristic of Microstructural Changes and Property Evaluation in Engineered Materials." (MS thesis). Retrieved from http://scholarcommon.sc.edu/etd

[42] Majumdar, P.K.; Clifford, J ; Haider, M. F.; Reifsnider, K. L. "Quantitative Description of Damage Evolution and Property Degradation of Fiber Reinforced Composite Materials.", *American Society for Composites 30th Technical Conference September* 28-30, 2015 Michigan State University, East Lansing, Michigan,USA.

[43] Huray P.G., (2010). *Maxwell's equation*, John Wiley & Sons, Inc. Hoboken, New Jersey

[44] Fleisch D., (2008). *A student's guide to Maxwell's equations*, Cambridge University Press, New York.

[45] https://en.wikipedia.org/wiki/Permittivity#cite_note-4

[46] Tuncer, E., Serdyuk, Y. V., and Gubanski, S. M. (2001). Dielectric mixtures--electrical properties and modeling. arXiv preprint cond-mat/0111254.

[47] Ogihara, S. and Reifsnider, K.L. (2002) "Characterization of nonlinear behavior in woven composite laminates." *Applied Composite Materials*, 2002. 9(4): p. 249-63

[48] Reifsnider, K., Case, S. and Duthoit, J. (2000) "The mechanics of composite strength evolution." *Composites Science and Technology*, 2000. 60(12-13): p. 2539-2546.

[49] Reifsnider, K.L. (1986) "The critical element model: A modeling philosophy." *Engineering Fracture Mechanics.* 1986. 25(5-6): p. 739-749.

[50] Torquato, S. (1985)"Effective electrical conductivity of two-phase disordered composite media". *J Appl Phys*, 58 (10) (1985), pp. 3790–3797

[51] Greenwood, J. .H.; Lebedat, S.; Bernasconi, J. (1975) "The anisotropic electrical resistivity of a carbon fibre reinforced plastic disc and its use as a transducer" *J Phys E Sci Instrum*, 8 (1975), pp. 369–370

[52] Kovacik, J. (1998) "Electrical conductivity of two-phase composite material" *Scri Mater*, 39 (2) (1998), pp. 153–157

[53] Louis, M., Joshi, S.P., Brockmann, W. (2001) "An experimental investigation of through-thickness electrical resistivity of COMPOSITES laminates,"

*Composites Science and Technology*, Volume 61, Issue 6, May 2001, Pages 911-919, ISSN 0266-3538

[54] Ezquerra, T.A ., Connor, M.T., Roy, S., Kulescza, M., Fernandes-Nascimento, J., Baltá-Calleja, F.J. (2001) "Alternating-current electrical properties of graphite, carbon-black and carbon-fiber polymeric composites", *Composites Science and Technology*, Volume 61, Issue 6, May 2001, Pages 903-909.

[55] Lin, Y., Gigliotti, M., Christine, M., Lafarie-Frenot, Bai, J., Marchand, D., Mellier, D. (2015)" Experimental study to assess the effect of carbon nanotube addition on the through-thickness electrical conductivity of CFRP laminates for aircraft applications," *Composites Part B: Engineering*, Volume 76, July 2015, Pages 31-37

[56] Makvandi, Resam, and Andreas Öchsner.(2014) "On a Finite Element Approach to Predict the Thermal Conductivity of Carbon Fiber Reinforced Composite Materials." *Defect and Diffusion Forum*. Vol. 354. 2014.